THE JOURNAL OF PHYSICAL CHEMISTRY A

Article

Benzo[c][1,2,5]thiadiazole Donor-Acceptor Dyes: A Synthetic, Spectroscopic and Computational Study

Jonathan E. Barnsley, Georgina E Shillito, Christopher Bryan Larsen, Holly van der Salm, Lei E. Wang, Nigel T. Lucas, and Keith C Gordon

J. Phys. Chem. A, **Just Accepted Manuscript** • DOI: 10.1021/acs.jpca.6b00447 • Publication Date (Web): 26 Feb 2016

ACS Publications

The Journal of Physical Chemistry A is published by the American Chemical Society. 1155 Sixteenth Street N.W., Washington, DC 20036

Benzo[*c*][1,2,5]thiadiazole Donor-Acceptor Dyes: A Synthetic, Spectroscopic and Computational Study

Jonathan E. Barnsley‡, Georgina E. Shillito‡, Christopher B. Larsen‡, Holly van der Salm, Lei E. Wang, Nigel T. Lucas*, Keith C. Gordon*

Department of Chemistry, University of Otago, P. O. Box 56, Dunedin, New Zealand

ABSTRACT: The synthesis, optical characterization and computational modelling of seven benzo[*c*][1,2,5]thiadiazole (**BTD**) donor-acceptor dyes are reported. These dyes have been studied using electrochemical analysis, electronic absorption, emission, Raman and resonance Raman spectroscopies coupled with various density functional theoretical approaches. Crystal structure geometries on a number of these compounds are also reported. The optical spectra are dominated by low energy charge-transfer states; this may be modulated by the coupling between donor and acceptor through variation in donor energy, variation of the donor-acceptor torsion angle, and incorporation of an insulating bridge. These modifications result in a perturbation of the excitation energy for this charge-transfer transition of up to ~2000 cm^{-1}. Emission spectra exhibit significant solvatochromisim, with Lippert-Mataga analysis yielding $\Delta\mu$ between 8 and 33 D. Predicted λ_{max}, ε and Raman cross-sections calculated by M06L, B3LYP, PBE0, M06, CAM-B3LYP and ωB97XD DFT functionals were compared to experimental results and analyzed using multivariate analysis, which shows that hybrid functionals with 20-27% HF best predict ground state absorption, whilst long-range corrected functionals best predict molecular polarizabilities.

INTRODUCTION

Organic donor-acceptor (D-A) dyes have been of significant interest in recent years as a result of potential applications in organic photovoltaics, dye-sensitized solar cells and non-linear optics.[1-4] Specifically, D-A dyes incorporating benzo[c][1,2,5]thiadiazole (BTD) have shown promise in these fields due to a low band gap and highly tunable optical properties.[5]

These tunable optical properties stem from charge-transfer (CT) transitions, which are typical for D-A dyes.[6,7] CT transitions result in a shift of electron density from the donor to the acceptor moiety and modulation of the coupling between the donor and acceptor allows fine control of photophysical properties.[8] Such systems result in partially zwitterionic excited states which can undergo solvent stabilization. Thus, variation of the solvent environment can also be utilized as a tuning mechanism.[9]

In the pursuit of specialized photophysical properties, intense electronic absorption in the visible region, for example, many predictive tools have been developed to identify promising synthetic targets.[10,11] One powerful and widely used approach is density functional theory (DFT). DFT provides a computationally efficient and reasonably accurate method to model chemical systems.[10,12] Despite its wide use, which DFT approach is most effective is subject to debate and varies significantly depending on the chemical system investigated or the target information.[10,12-15]

Various computational approaches exist, including 'pure' functionals and hybrid methods (such as B3LYP). 'Pure' methods calculate exchange and correlation terms by implementing electron density approximations (LDA/GGA), while hybrid methods combine 'pure' calculations with exact exchange energies calculated by Hartree-Fock theory (HF). These hybrid methods fall into two categories (global and range separated) based on the evolution of HF exchange over electron-electron distance.[16] The fundamental differences in how these functionals predict geometries and photophysical properties consequently afford functional-dependent results, can compromise the understanding of these promising systems.

There have been a number of studies investigating computational predictions of photophysical properties in donor acceptor-dye systems.[17-27] In the case of this study, particular attention is paid to the influence of HF, and functionals are specifically picked based on their common/wide use in donor-acceptor studies. The inclusion of experimental and calculated Raman cross-sections provides additional testing of the calculations via experimental data.

Herein we report a series of seven D-A BTD dyes with varying degrees of steric bulk so as to conformationally control the D-A torsion angle. Also included

are several permutations of the D-A framework to investigate linker and donor effects. The dependence of optical properties on solvent is investigated both experimentally (with optical/vibrational spectroscopies) and theoretically (with a DFT calculation library, using six different functionals with different levels of HF exchange, M06L - 0%, B3LYP - 20%, PBE0 - 25%, M06 - 27%, CAM-B3LYP - 19-65% and ωB97XD - 22-100%, with five different solvents). In order to identify possible correlation these data are subjected to principal component analysis (PCA).

RESULTS AND DISCUSSION

Compounds Investigated

For this study the compound series is based on a benzothiadiazole-triphenylamine (**BTD-TPA**) framework (**Figure 1**). Addition of substituents to either the adjacent site to the TPA unit (as in **BTDMe-TPA** or **BTD-TPA$_2$**) or to the phenyl ring of the substituent (as in **BTD-(OMe)$_2$TPA** and **BTD-(OMe)$_2$Ph**) should cause an increase in the donor-acceptor torsion angle due to steric factors. However, the methoxy group in particular may also have electronic effects.[28,29] **BTD-(OMe)$_2$Ph** lacks an amine donor, and is included as a control for the influence of the methoxy-groups.

The other compounds investigated are altered in different ways; a 'click' triazolyl bridge is included (**BTD-TRZTPA**), the donor group is changed from TPA to Ph-NMe$_2$ (**BTD-NMe$_2$**) and an additional donor group is added (**BTD-TPA$_2$**) which alters both $\varphi_{D\text{-}A}$ and the electronic properties of the donor.

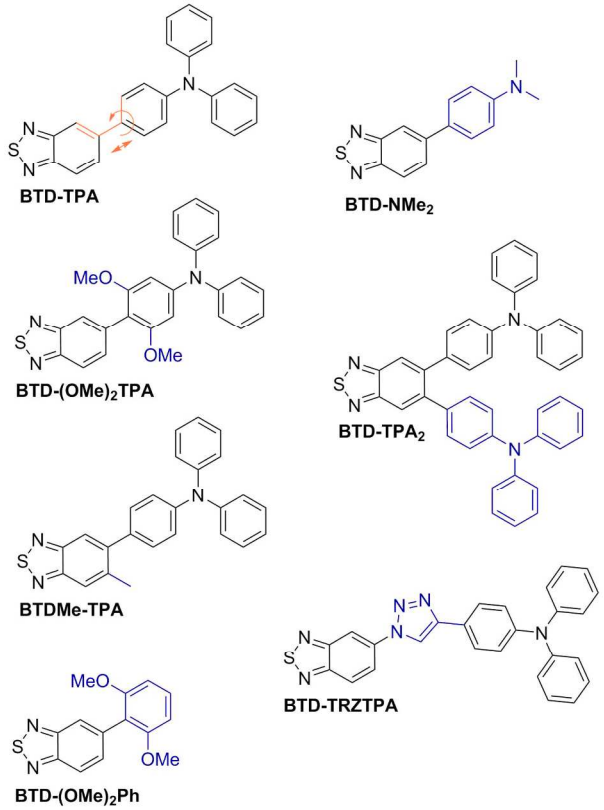

Figure 1. The compound series studied in this work, showing $\varphi_{D\text{-}A}$/bond length of the parent **BTD-TPA** in orange, and the subsequent variations in blue.

Synthesis and Characterization

The synthesis of the target compounds is presented in Scheme 1. **BTD-(OMe)$_2$Ph**, **BTD-NMe$_2$** and **BTD-TPA** are prepared in one high-yielding step from 5-bromobenzo[*c*][1,2,5]thiadiazole (**BTD-Br**) using Suzuki-Miyaura couplings with the appropriate substituted boronic acid. **BTD-TPA$_2$** is likewise prepared in one high-yielding step from 5,6-dibromobenzo[*c*][1,2,5]thiadiazole (**BTD-Br$_2$**) using Suzuki-Miyaura coupling.

Incorporation of methoxy groups on the TPA donor was achieved by preparing an appropriately substituted phenylboronic acid incorporating a masked halide in the form of a trimethylsilyl group. This useful building block was achieved in two high-yielding steps from commercially available 1-bromo-3,5-dimethoxybenzene. The first step involves protecting the bromo group site as a trimethylsilyl group through lithiation and reaction with Me_3SiCl. The second step involves *ortho*-lithiation and subsequent borylation selectively at the position flanked by the methoxy groups. An X-ray crystal structure of the product (**Figure 2**) shows intermolecular hydrogen-bonding between the boronic acid protons and the methoxy group oxygens. This is a rare case in which boronic

acid protons are 'tethered' through intramolecular hydrogen-bonding,[30] permitting purification through preparative column chromatography. Suzuki-Miyaura coupling between this substituted phenylboronic acid and **BTD-Br** proceeds in excellent yield. Deprotection of the masked halide through iododesilylation proceeds in good yield at low temperatures, then Buchwald-Hartwig coupling *N*,*N*-diphenylamine affords **BTD-(OMe)$_2$TPA** in moderate yield.

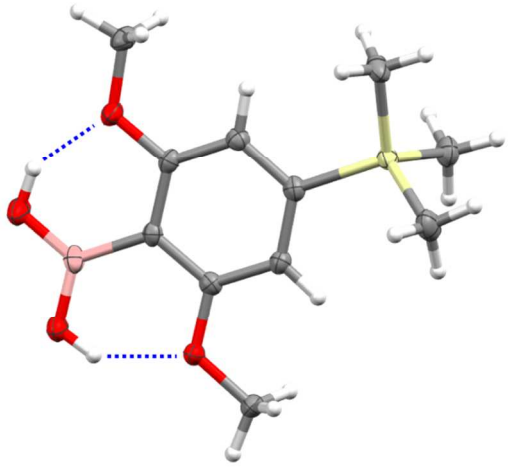

Figure 2. X-ray crystal structure of 4-trimethylsilyl-2,6-dimethoxyphenylboronic acid with ellipsoids depicted at the 50% probability level. Intermolecular hydrogen-bonding is depicted with blue dashed lines.

Incorporation of a methyl group on the BTD acceptor was achieved through the preparation of an analogue of **BTD-Br**, namely 5-bromo-6-methylbenzo[*c*][1,2,5]thiadiazole (**BTDMe-Br**). This was accomplished in four steps from commercially available 4-methyl-1,2-phenylenediamine. The first step involves protection of the amines with TsCl in near quantitative yield. The sterically bulky Ts groups protect the 3- and 6- positions from substitution; bromination occurs selectively at the 5-position. Deprotection of the amines with H_2SO_4, followed by NaOH neutralization, affords the corresponding 1,2-phenylenediamine in good yield and subsequent reaction with $SOCl_2$ affords the BTD in excellent yield. Suzuki-Miyaura coupling with 4-diphenylaminophenylboronic acid affords **BTDMe-TPA** in good yield.

BTD-TRZTPA was prepared in two steps from 5-aminobenzo[*c*][1,2,5]thiadiazole. Diazotization of the amino group and *in situ* conversion to the azide proceeds in average yields, followed by CuAAC "click" reaction of the azide with 4-ethynyl-*N*,*N*-diphenylaniline in excellent yield.

X-ray crystal structures were obtained for **BTD-NMe$_2$**, **BTD-TPA**, **BTD-TPA$_2$** and **BTD-(OMe)$_2$TPA**, using crystals obtained from EtOH recrystallizations. **BTD-NMe$_2$** crystallized in the *Pbca* space group, **BTD-TPA** in the $P2_1/c$ space group, **BTD-TPA$_2$** in the P*bcn* space group and **BTD-(OMe)$_2$TPA** in the *P*-1 space group. In all cases the BTD unit is completely planar, and the amine donor relatively planar, with N3 lying 0.10, 0.02, 0.02 and 0.00 Å, respectively, above a plane defined by the *ipso* carbons (*ipso* carbon and methyl groups for **BTD-NMe$_2$**). The donor unit is rotated 9.7°, 26.7°, 53.4° and 47.9°, respectively, from the BTD acceptor. For **BTD-TPA**, **BTD-TPA$_2$** and **BTD-(OMe)$_2$-TPA**, terminal donor phenyl rings are rotated from the donor phenylene with torsion angles of -31.8° and 128.4° for **BTD-TPA**, -49.4° and 74.1° for **BTD-TPA$_2$**, and -40.3° and 140.4° for **BTD-(OMe)$_2$TPA**, which also has the methoxy groups in plane with the donor phenylene.

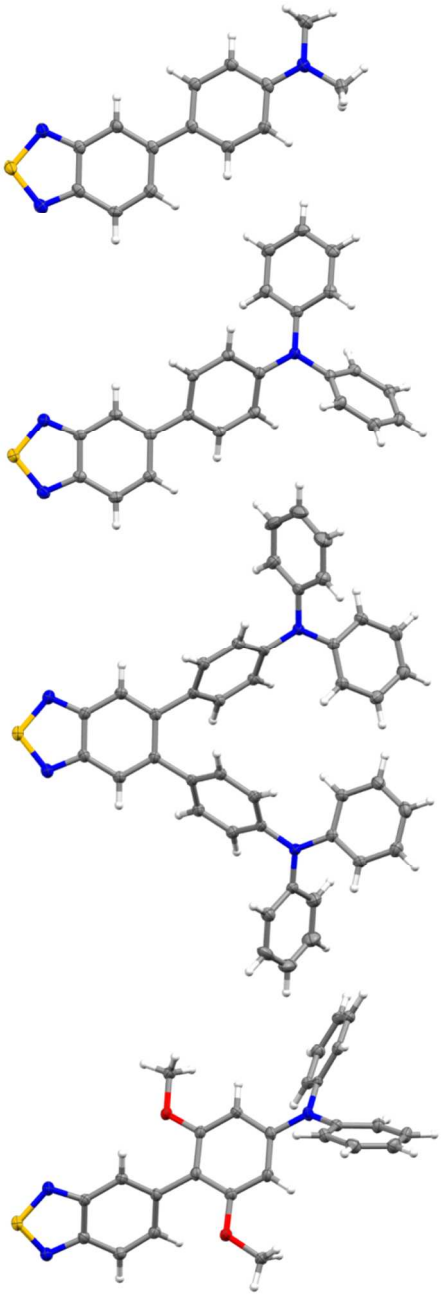

Figure 3. X-ray crystal structures obtained for **BTD-OMe$_2$Ph**, **BTD-TPA**, **BTD-TPA$_2$**, **BTD-OMe$_2$TPA**. Ellipsoids are shown at the 50% probability level.

Ground-State Geometries

Donor-acceptor torsion angles ($\varphi_{D\text{-}A}$) and bond lengths ($r_{D\text{-}A}$) obtained from DFT geometry optimizations and X-ray crystal structures are presented in **Table 1**. DFT geometry optimizations yield partially twisted structures around the D-A bond: **BTD-TRZTPA** was predicted to possess the smallest calculated angle (-21.4° to -33.0°) through to **BTD-(OMe)$_2$Ph** with the largest (51.7° to 61.4°). The **BTD-TRZTPA** structure results from minimal steric bulk and an electron rich π system that favors planarity, while **BTD-(OMe)$_2$Ph** possesses maximal steric bulk with minimal ability to share π electrons due to the absence of a donor group. In the case of the remaining compounds, the trend in $\varphi_{D\text{-}A}$ is consistent with steric bulk; **BTD-NMe$_2$** < **BTD-(OMe)$_2$TPA** < **BTDMe-TPA** < **BTD-TPA$_2$**. Whilst it might be expected that the methoxy groups perturb the electronic nature of the TPA donor,[28,29] electrochemical studies show E_{ox} of **BTD-(OMe)$_2$TPA** and **BTD-TPA** (**Table S1**) to be virtually unchanged by methoxy substitution.

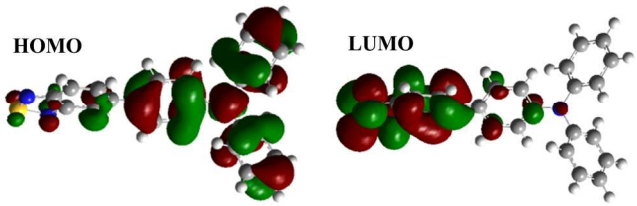

Figure 4. DFT-calculated HOMO and LUMO orbitals for **BTD-TPA** in acetonitrile using the B3LYP functional. Calculated orbitals for the remaining compounds can be found in **Figure S16**.

The choice of functional has an effect on the absolute calculated value which exemplifies the role that functionals play in computational results. For M06L, with no HF or orbital exchange contribution, the absolute angle for all compounds is calculated to be the smallest (-28.2° for **BTD-TPA**). As the contribution of HF is increased from left to right across **Table 1** (0%, 20%, 25%, 27%, 19-65% and 22-100%, respectively) there is an increase of $\varphi_{D\text{-}A}$ up to -38.8° for **BTD-TPA** using ωB97XD. Typically, equilibrium geometries are predicted much more effectively by pure or global hybrids with small HF contributions.[31] A plausible explanation for this is that the short range nature of covalent bonds, where most of the stabilization results from local electron interaction; this is observed, with M06L most accurately and ωB97XD least accurately replicating experimental results. Deviations between calculated and experimental angles are attributed to calculations not accounting for solid-state packing interactions observed in the crystal.

Scheme 1. Synthesis of target compounds.

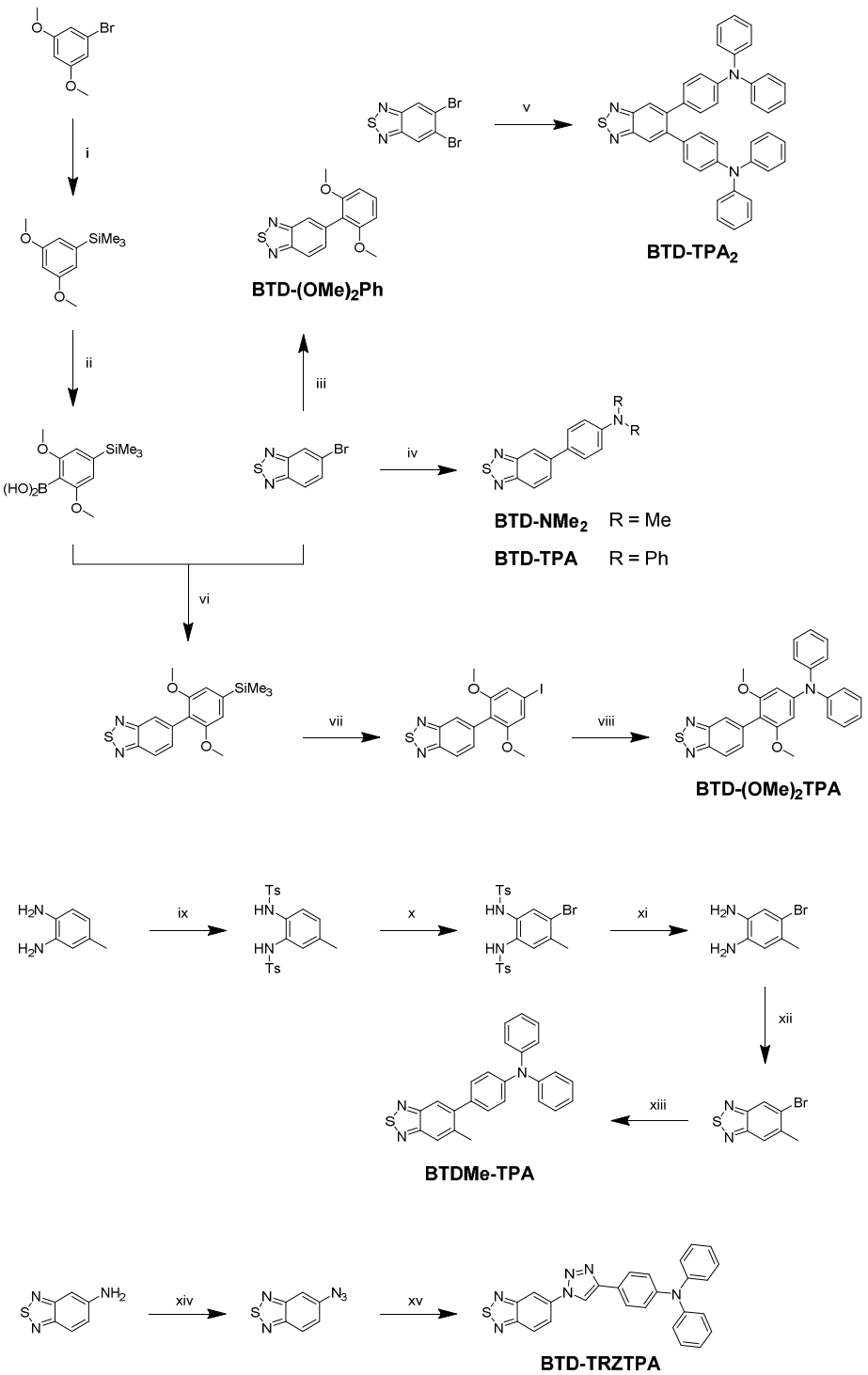

(i) a. *n*-BuLi, THF, -78 °C, 2 h, b. Me_3SiCl, rt, 15 h, 97%; (ii) a. *n*-BuLi, THF, 0 °C, 15 h, b. $B(OMe)_3$, rt, 5 h, c. aq. NH_4Cl (sat.), rt, 2 h, 69%; (iii) 2,6-dimethoxyphenylboronic acid, K_2CO_3, $PdCl_2$(dppf), toluene, water, EtOH, reflux, 15 h, 87%; (iv) 4-dimethylaminophenylboronic acid or 4-diphenylaminophenylboronic acid, K_2CO_3, $PdCl_2$(dppf), toluene, water, EtOH, reflux, 15 h, 75% (R = Me), 94% (R = Ph); (v) 4-diphenylaminophenylboronic acid, K_2CO_3, $PdCl_2$(dppf), toluene, water, EtOH, reflux, 15 h, 80%; (vi) K_2CO_3, $PdCl_2$(dppf), toluene, water, EtOH, reflux, 15 h, 96%; (vii) ICl, CH_2Cl_2, -78 °C, 2 h, 80%; (viii) diphenylamine, *t*-BuOK, [*t*-Bu_3PH]BF_4, Pd_2(dba)$_3$, toluene, reflux, 15 h, 50%; (ix) TsCl, py, CH_2Cl_2, rt, 3 h, 95%; (x) Br_2, AcONa, AcOH, reflux, 3 h, 91%; (xi) a. conc. H_2SO_4, reflux, 3 h, b. NaOH, 87%; (xii) $SOCl_2$, NEt_3, CH_2Cl_2, reflux, 15 h, 90%; (xiii) 4-diphenylaminophenylboronic acid, K_2CO_3, $PdCl_2$(dppf), toluene, water, EtOH, reflux, 15 h, 80%; (xiv) TsOH, $NaNO_2$, NaN_3, CH_3CN, water, rt, 2 h, 20%; (xv) 4-ethynyl-*N*,*N*-diphenylaniline, L-ascorbic acid, $CuSO_4 \cdot 5H_2O$, DMF, H_2O, rt, 15 h, 91%

Table 1. Calculated $\varphi_{D\text{-}A}$ and bond lengths. Data shown are calculated with an acetonitrile solvent field.

	$\varphi_{D\text{-}A}$ / ° ($r_{D\text{-}A}$ /Å)						
	M06L	B3LYP	PBE0	M06	CAM-B3LYP	ωB97XD	Crystallography
BTD-TPA	28.2(1.43)	34.0 (1.48)	34.3(1.48)	35.0 (1.47)	36.0(1.48)	38.8(1.49)	26.7(1.49)
BTD-$(OMe)_2$TPA	48.2(1.48)	54.0(1.49)	52.1(1.49)	53.1 (1.48)	54.1 (1.48)	57.4(1.49)	47.9(1.49)
BTDMe-TPA	43.4(1.47)	55.8(1.49)	55.3(1.48)	52.3 (1.48)	58.1(1.50)	59.7(1.49)	-[a]
BTD-TPA_2	46.9(1.49)	49.3(1.49)	48.0 (1.49)	50.9 (1.48)	50.6(1.48)	56.1(1.49)	53.4 (1.49)
BTD-NMe_2	26.7(1.47)	31.0(1.48)	31.5(1.47)	31.8 (1.47)	33.3(1.48)	35.7 (1.48)	9.7(1.49)
BTD-TRZTPA	21.4(1.41)	29.0(1.42)	29.5 (1.41)	25.9(1.42)	30.5(1.42)	33.0(1.42)	-[a]
BTD-$(OMe)_2$Ph	51.7(1.48)	57.5(1.49)	55.7(1.48)	55.4(1.48)	56.9(1.49)	61.4 (1.49)	-[a]

[a] Dashes indicate compounds which failed to afford quality crystals for X-ray crystallography.

Ground-State Vibrational Spectroscopy

Mean absolute deviations (MADs) can be used to understand how effectively an optimized geometry models the compound in question. MADs for this study were calculated as explained by Earles *et al.*[32] A MAD of around 10 cm^{-1} is considered satisfactory and low HF functionals such as M06L and B3LYP overall provide satisfactory MADs (13 and 10 cm^{-1} respectively, **Table 2**) while range separated HF functionals CAM-B3LYP and ωB97XD are considerably less accurate at calculating vibrational frequencies for these compounds (average MADs of 27 and 25 cm^{-1} respectively). Vibrational frequencies are dependent on the ground-state bonding networks, which as stated above, are more accurately modelled in low HF hybrid functionals.

Differential Raman cross-sections in acetonitrile and toluene were evaluated for each compound. Raman cross-sections probe the overall polarizability of a molecule, which is affected by conjugation.[33] These are presented in **Table S4**. In order to compare these complex series the calculated normal modes were examined and it was possible to identify modes that are BTD-based, TPA-based and delocalized. This is exemplified by the Raman spectrum of BTD-TPA (**Figure 5**). Modes at 1179 cm^{-1} and 1278 cm^{-1} are TPA localized, while 1217 cm^{-1} is a BTD band and the strongest bands at 1597 and 1612 cm^{-1} are of mixed origin. The mixed modes have the largest differential Raman cross sections, ranging from 2 to 40 cm^2 sr^{-1} $molecule^{-1}$ and are typically 50 to 75% more intense than the localized TPA and BTD modes.

Figures S3-S10 detail significant variation in the predicted Raman cross section values, which are affected by both the functional used and the solvent field. For example BTD-TPA has a considerable spre. In acetonitrile, the absolute value for the cross section is considerably overestimated by non-hybrid and global hybrid functionals (400% for M06L, **Table 3**), while long-range corrected functionals were more accurate (-0.77% for ωB96XD). This result appears sensible in the view that long-range corrected functionals (e. g. ωB97XD), model long distance electron interactions more effectively than non-hybrid and global hybrid functionals, and would therefore be expected to more effectively model the polarizability, a property which depends on electron density across the whole molecule.[10] There appears to be no consistent error associated with TPA, BTD and mixed modes in these cases.

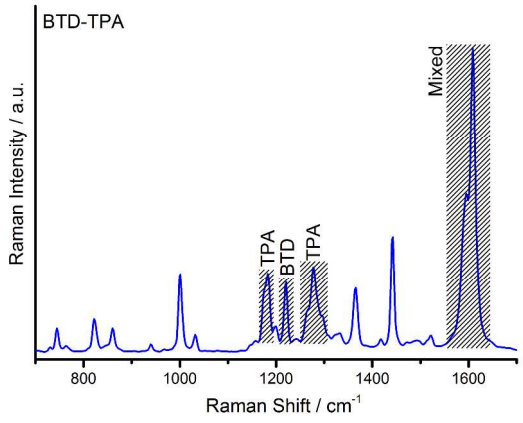

Figure 5. FT-Raman spectra of neat BTD-TPA collected at 1064 cm^{-1}.

Table 2. Mean absolute deviations (MADs) for calculated Raman frequencies in acetonitrile.

	Mean Absolute Deviation of Raman Modes / cm^{-1}					
	M06L	B3LYP	PBE0	M06	CAM-B3LYP	ωB97XD
BTD-TPA	17	10	22	13	32	34
BTD-$(OMe)_2$TPA	10	10	18	16	25	23
BTDMe-TPA	10	9	23	15	39	31
BTD-TPA_2	11	13	17	13	23	23
BTD-NMe_2	16	10	15	12	19	17
BTD-TRZTPA	18	8	19	17	26	26
BTD-$(OMe)_2$Ph	8	12	15	14	23	21
Average	13	10	18	14	27	25

Table 3. Mean percentage errors for calculated Raman cross sections of BTD-TPA when compared to experimental data.

	Mean percentage error in calculated Raman cross section /%					
	M06L	B3LYP	PBE0	M06	CAM-B3LYP	ωB97XD
Acetonitrile	400	298	176	148	4.14	-0.770
Toluene	195	49.2	46.5	77.0	-51.3	-40.3

Electronic Absorption Spectroscopy

Previously investigated D-A compounds using a BTD acceptor show a series of optical transitions; the lowest energy band is typically of CT character, while higher energy transitions tend to be of π-π* character.[34-36] Optical data of this lowest energy transition for the investigated compounds are presented in **Table 4**. It appears that as $\varphi_{D\text{-}A}$ is increased, the absorption band energy increases and intensity decreases. This is exemplified by **BTD-TPA**, which has one of the smallest calculated $\varphi_{D\text{-}A}$ (-28.1° to -38.80°) and exhibits the lowest energy (399 nm) and one of the most intense transitions (12600 M^{-1} cm^{-1}) of the TPA-containing dyes. Such results support the assignment of this low energy band as CT, since $\varphi_{D\text{-}A}$ affects conjugation or communication between donor and acceptor groups, which consequently perturbs both the optical transition energy and allowedness of a transition. DFT results for **BTD-$(OMe)_2$TPA** and **BTDMe-TPA** correctly predict decreases in λ_{max} and ε as a result of an increased $\varphi_{D\text{-}A}$.

The inclusion of triazole results in a blue shift of the low energy band by 2260 cm^{-1} and a decrease of nearly 30% in extinction coefficient when compared to **BTD-TPA**. This indicates a decrease in communication between donor and acceptor similar to that due to an increase in $\varphi_{D\text{-}A}$ as for **BTDMe-TPA**, consistent with the triazole acting as an electronically insulating bridge. Computational chemistry supports these findings with vast decreases in CT band intensity for all functionals except ωB97XD.

Table 4. Experimental and calculated absorption data for the lowest energy transition. All data were collected or modelled in acetonitrile.

	λ_{max} /nm (ε /M^{-1} cm^{-1})	Absorption Max λ_{max} /nm (Oscillator Strength)					
	EXPERIMENTAL	M06L	B3LYP	PBE0	M06	CAM-B3LYP	ωB97XD
BTD-TPA	399(12600)	686(0.19)	527(0.23)	480(0.26)	469(0.27)	354(0.52)	335(0.56)
BTD-$(OMe)_2$TPA	382(9000)	680(0.12)	519(0.14)	472(0.18)	459(0.18)	349(0.35)	332(0.37)
BTDMe-TPA	371(9330)	687(0.11)	515(0.09)	466(0.10)	455(0.13)	330(0.27)	312(0.27)
BTD-TPA_2	398(10300)	713(0.21)	541(0.19)	492(0.23)	479(0.24)	349(0.58)	328(0.64)
BTD-NMe_2	408(16800)	621(0.21)	510(0.25)	472(0.27)	462(0.27)	362(0.40)	345(0.40)
BTD-TRZTPA	366(9100)	886(0.03)	581(0.03)	512(0.04)	493(0.04)	329(0.30)	307(0.70)
BTD-$(OMe)_2$Ph	315(10900)	457(0.11)	396(0.06)	371(0.12)	373(0.12)	316(0.15)	309(0.12)

BTD-NMe_2 provided the most intense (16800 M^{-1} cm^{-1}) and lowest energy (408 nm) band of all compounds. This is a result of a small calculated $\varphi_{D\text{-}A}$ and the donor NMe_2 group being a stronger donor than TPA, as evidenced by electrochemistry (**Table S1**).The addition of a second TPA group in **BTD-TPA_2** resulted in a decrease in extinction coefficient but negligible change to the λ_{max}. The addition of the second TPA results in both donor groups twisting out of plane relative to BTD, changing $\varphi_{D\text{-}A}$ significantly. The blue shift expected with an increased $\varphi_{D\text{-}A}$ is offset by the presence of a second donor. This results in an overall small net change. The decrease of intensity resulting from a second TPA group is only predicted for functionals B3LYP, PBE0 and M06, which also predict a small red-shift for the transformation. In **BTD-$(OMe)_2$Ph** there is an absence of the CT transition as a result of lacking a strong donor group.

Resonance Raman spectra were collected at 351 nm, which probes the lowest energy transition. Resonance Raman spectra show selective enhancement of vibrational modes associated with the active chromophore, which helps elucidate the transition nature.[37] More specifically, modes that 'mimic' changes due to a excitation to an excited state, such as CO stretching for MLCT transitions, are typically enhanced on the order of 10^4 to 10^5.[38] In this case, spectra show the enhancement of a number of BTD and TPA modes (**Figure S15**), which would be expected for a shift of electron density from TPA to BTD.

TD-DFT data (**Table 4**), shows a significant increase in transition energy and oscillator strength for the CT transition with an increase in HF contribution to the calculation. For BTD-TPA there is an increase of >15,000 cm^{-1} (51%) in transition energy and an increase of >66% in oscillator strength when calculated with wB97XD compared to M06L. This difference is a result of the lack of sensitivity to long-range interactions in low HF methods, resulting in an underestimation of oscillator strength and excitation energy.[31,39,40] A small part of this change is likely to be a result of the increased $\varphi_{D\text{-}A}$ present in geometry optimization, but this is minor compared to fundamental differences in the nature of these functionals.

Long-range corrected functionals (CAM-B3LYP and wB97XD) correctly predict the λ_{max} experimental trend within the compound series, while the functionals B3LYP, PBE0 and M06 correctly predict the *f* trend. The ability to predict these trends is powerful; DFT calculated absolute values, however, are considerably less meaningful. **Figure S13** shows that high HF calculations (wB97XD) fail to account for any solvent effects in these compounds, while M06L is much better and predicts a stabilization of the ground state (HOMO) in polar solvents like acetonitrile.

It is pertinent to not only investigate the predicted energy and oscillator strengths of transitions but also at the orbital contributions for said transitions. In most cases the lowest energy transition is predicted to be HOMO to LUMO in nature (**Figure 4**) which represents a CT transition since the HOMO is TPA-based and the LUMO BTD-based. Long-range corrected functionals (CAM-B3LYP and wB97XD) also predict considerable orbital contribution from other donor

orbitals (HOMO-1, HOMO-2 and HOMO-3). These orbitals are significantly delocalized, causing the calculated transitions to become more π-π* in nature – explaining a higher predicted transition energy.

Figure 6 shows frontier molecular orbital (FMO) energies estimated from experimental techniques and calculated using two different functionals. Experimental HOMO and LUMO energies are estimated from cyclic voltammetry data using previously established methods (**Table S1**).[41]

The agreement between values obtained from electrochemistry and PBE0 calculations is within 20%. Using wB97XD the level of agreement becomes nearly 50%. The LUMO energies obtained electrochemically and from PBE0 calculations show good agreement, suggesting the LUMO is modelled well using this functional. As the amount of orbital exchange in the functional increases, the HOMO is predicted to be increasingly stabilised, while the LUMO is increasingly destabilized.

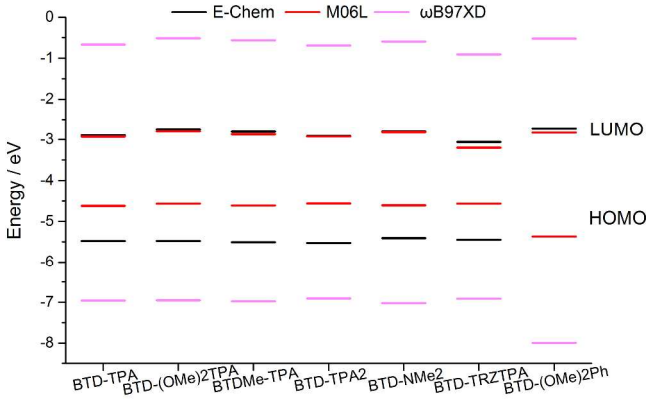

Figure 6. Calculated frontier molecular orbital energies for experimental and computational data. All data were collected or modelled in dichloromethane. A full FMO diagram can be found in SI (**Figure S14**).

Emission Spectroscopy

Emission spectra show solvatochromism (**Figure 7a**). For **BTD-TPA**, the emission wavelength varies by ~5000 cm^{-1}, from 502 nm in toluene to 673 nm in acetonitrile. This behavior arises due to an excited state which is more polarized than the ground state, and therefore is more stabilized by more polar solvents.[9] **BTD-TPA** shows dual emission in acetonitrile, with the higher energy state likely to be of π,π* origin.

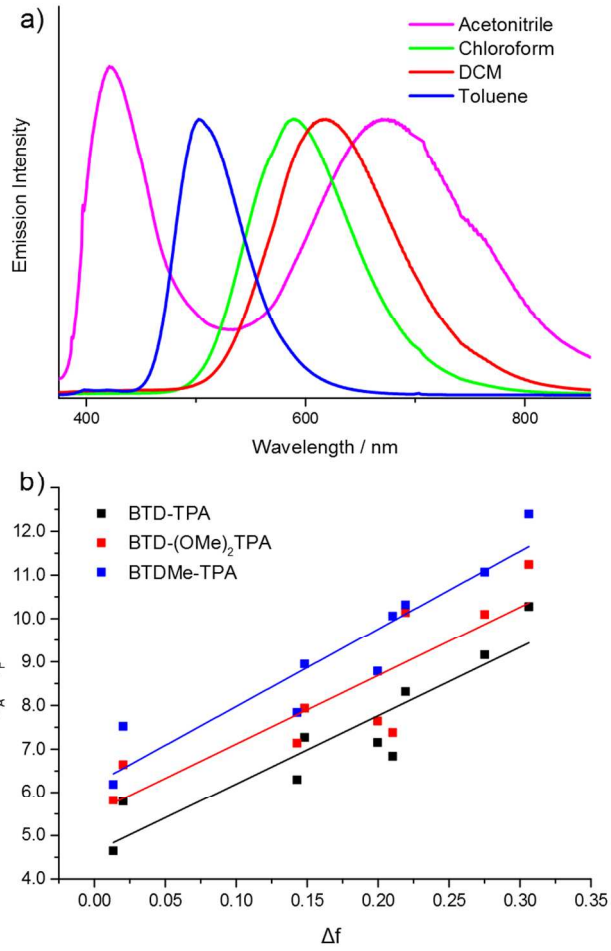

Figure 7. (a) Emission data for **BTD-TPA** in a number of solvents and (b) a Lippert Mataga plot for **BTD-TPA**, **BTD-OMe$_2$TPA** and **BTD-MeTPA**.

Using the Lippert-Mataga equation, the relationship between the Stokes shift and solvent polarity parameter can be related to a change in dipole moment between the ground and emissive excited states (Δμ, **Figure 7b**).[9]

For dyes with a similar r_{D-A}, and therefore similar Onsager radii, the Δμ value is around 21-22 D which indicates significant charge transfer (**Table 5**). **BTD-NMe$_2$** has a smaller Onsager radius, and a smaller calculated Δμ of 15 D while **BTD-TRZTPA** which has a larger Onsager radius is calculated to have a Δμ of 33 D, considerably more than the other compounds. **BTD-OMe$_2$Ph** shows emission from a π* state, not a CT state as for the other compounds. The electron density of the HOMO and LUMO orbitals can still be localized, resulting in a net Δμ.

Table 5. Lippert Mataga data for the compound series.

Compound	Δμ /D
BTD-TPA	22
BTD-OMe_2TPA	22
BTD-MeTPA	21
BTD-TPA_2	21
BTD-NMe_2	15
BTD-TRZTPA	33
BTD-OMe_2	8

Mean Percentage Error (MPE) Analysis

To investigate the effectiveness of the different functionals to predict both structural and electronic properties of this compound series, MPEs have been calculated by comparing calculated DFT results to experimental data. Parameters include λ_{max} (cm^{-1}), ε, and cross sections for five Raman vibrations present in all compounds, across solvent and functional.

Figure 8 shows Raman cross sections are significantly overestimated by nearly all functionals and the extent of error is considerably more than for the absorption max and extinction coefficient. As discussed previously, non-hybrid and global hybrid functionals considerably overestimate the polarizability of this dye series (over 320% for M06L, **Table 6**) whilst the long-range corrected functionals are more accurate (<±25%). The long-range corrected functionals overestimate the absorption energy and extinction coefficient for calculated transitions whilst the non-hybrid and global hybrid functionals underestimate these properties. In this case, M06 (27% HF) yields the smallest error across solvent and compound (-19.77%). Of particular note is the vast variation in error for the five cross-sections. **Figure S20** displays the predicted origin for each vibration. Cross-sections 1 and 3 (TPA based) are well predicted in terms of intensity, with cross-sections 4 and 5 (delocalized) somewhat well predicted, while cross-section 2 (BTD based) is vastly over estimated. This result indicates complexity in vibrational predictions, such that vibrations of differing nature result in differing degrees of overestimation. In the case of the BTD unit and its associated vibrations, most functionals performed poorly, especially that of the low HF functionals (M06L, B3LPY, and PBE0).

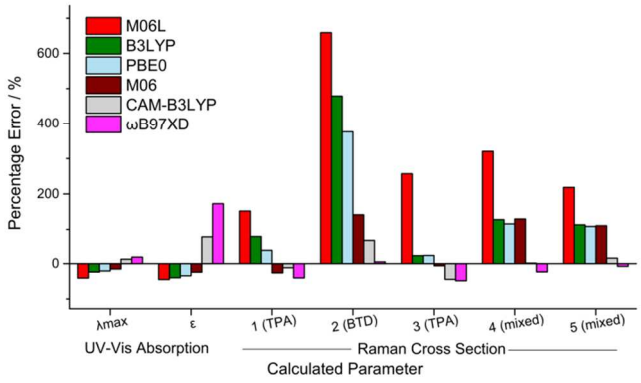

Figure 8. Mean percentage errors for each functional when compared to experimental data.

Table 6. Overall mean percentage error for absorption and Raman data; UV-Vis refers to a mean error associated to both λ_{max} and ε, where Raman refers to error in Raman cross sections.

	UV-Vis /%	Raman/ %
M06L	-43.1	321
B3LYP	-32.1	164
PBE0	-27.5	133
M06	-19.8	69.7
CAM-B3LYP	45.9	5.96
ωB97XD	95.5	-23.2

Principle Component Analysis

Principal component analysis (PCA) factorizes variation within a data set into a series of principal components. This technique is used to extract patterns from the data set that may have gone unnoticed by other analyses.[42] For this analysis the optical properties (λ_{max}, ε) were examined along with Raman cross-sections for five bands from each sample; two TPA based, two mixed and one BTD based. Analysis of the spectral and Raman data results in two PCs describing 78% of all data variance. The loadings plots give some insight into the relationship between different parameters.

PC1 is positively correlated with ε and negatively correlated to λ_{max} and all of the Raman cross sections as seen in **Figure 9b**. The inverse relationship between ε and λ_{max} originates from computational trends where increased energy of absorption is strongly associated with an increased extinction co-efficient (ε). Functionals that predicted a high energy transition also predicted modest Raman cross-sections. Cross sections 1 and 3 appears to behave slightly differently from the remaining cross sections as seen in PC1 and PC2 (**Figure S21).** This is believed to result from a nearly exclusive TPA

contribution to these stretches. In compounds such as **BTD-NMe$_2$**, **BTD-OMe$_2$Ph** and **BTD-TPA$_2$** the predicted intensity for these bands is lower than for **BTD-TPA**, this especially so for cross section 1.

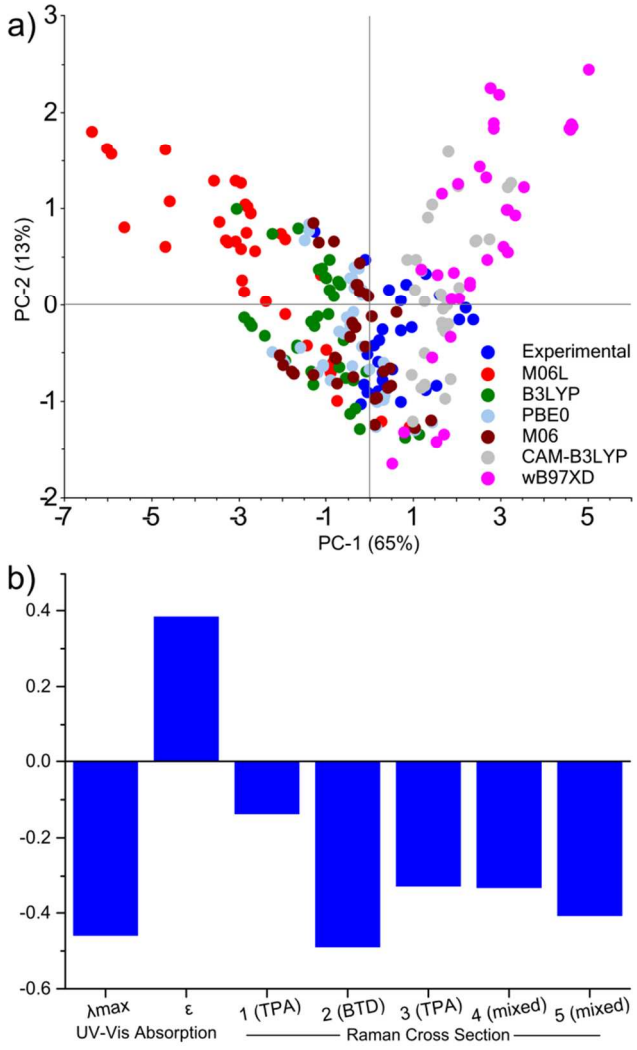

Figure 9. a) PCA scores plot for all compounds and solvents, distinguished by functional and b) PC1 loadings plot which describes 65% of variation within the data set.

Figure 9a presents PC1 (65% variation) and PC2 (13% variation) with an identical parameter set used for MPE analysis. The dispersed nature of data points is a visual reminder of the variability of computational chemistry. Experimental data clusters close to the origin, the closer functionals group to experimental data, the more effective the prediction. Whist there is mixing between clusters, M06L and B3LYP functionals can be separated from long-range corrected functionals (ωB97XD and CAM-B3LYP) as the former have negative PC1 scores and latter positive PC1 scores. What is powerful about PCA is the ability to 'see' how closely the functionals mimic the experimental data and where calculations fail. M06 best approximates experimental data with an overall slight underestimation of ε and an overestimation of both λ_{max} and α. This finding provides evidence that functionals with HF contributions close to 27% are suited for investigating the photo-physical properties of donor-acceptor dyes of similar nature to those studied here. At this point is in unclear how general these findings are. Although valid for these systems, further investigation is warranted to ascertain if our conclusions are appropriate for different donor-acceptor compounds and how applicable these strategies may be to other types of compounds.

CONCLUSIONS

The synthesis and characterization of seven benzo[c][1,2,5]thiadiazole donor-acceptor dyes has been reported. A broad absorption band is observed between 350 and 410 nm, and shown to be charge-transfer in nature from the TPA group to BTD using resonance Raman spectroscopy; DFT calculations using any of the functionals discussed herein are consistent with this. The energy and intensity of this transition is decreased by an increase in the torsion angle between donor and acceptor units or with the inclusion of an insulating linker group. Emission spectra show significant solvatochromism, with large values calculated using Lippert-Mataga analysis.

DFT calculations using a number of functionals with different HF exchanges were investigated in terms of their ability to accurately predict experimental properties. Data suggests that absorption properties (energy and ε) were predicted best using M06, while the molecular polarizability and therefore Raman cross-section were predicted best using hybrid functionals with long-range corrected Hartree-Fock exchange.

EXPERIMENTAL

General Experimental

5-bromobenzo[*c*][1,2,5]thiadiazole, 5,6-dibromobenzo[*c*][1,2,5]thiadiazole, 5-aminobenzo[*c*][1,2,5]thiadiazole and 4-ethynyl-*N*,*N*-diphenylaniline were prepared using literature procedures.[43-45] Commercially available reagents and solvents were used as received. Sigma-Aldrich spectroscopic or HPLC grade solvents were used for all spectroscopic measurements. Spectral data were analyzed using GRAMS A/I (ThermoScientific) and OriginPro v9.0 (Origin Lab Corporation). Numbering schemes for NMR assignments are presented in **Figure S23**.

Computational Methods

Geometry and vibrational calculations were generated using the Gaussian 09W program package which implemented M06L, B3LYP, PBE0, M06, CAM-B3LYP

and wB97XD functionals employing the basis set 6-31G(d).[46] Calculated gas phase vibrational spectra were generated using Gaussum v2.2.5 software, and scaled to give the lowest value for the mean absolute deviation for band position from experimental data with scale factors typically around 0.975.[47] TD-DFT calculations were also implemented, using the same functionals and basis set. molecular orbitals were visualized using Gauss View 5.0 W (Gaussian Inc.) while vibrations were visualized using Molden.[48]

Physical Measurements

^{1}H NMR spectra were recorded at 500 MHz and ^{13}C at 126 MHz on a Varian 500AR spectrometer. All samples were recorded at 25 °C in 55 mm diameter tubes. Chemical shifts were referenced internally to residual non-perdeuterated solvent using δ values as reported by Gottlieb *et al.*.[49] Chemical shifts are rounded to the nearest 0.1 Hz. Assignment of signals is assisted through the use of 2D NMR techniques (COSY, NOESY, ^{1}H-^{13}C HSQC and ^{1}H-^{13}C HMBC), recorded on a Varian 500AR spectrometer using standard pulse sequences. HR-ESI-MS was performed on a Bruker MicrOTOF-Q mass spectrometer operating in positive mode. Values are quoted as *m/z* ratio, with an instrumental uncertainty of *m/z* ±0.003. Analysis of elemental composition was made by the Campbell Microanalytical Laboratory at the University of Otago, using a Carlo Erba 1108 CHNS combustion analyzer. The estimated error is the measurements in ±0.4%.

For X-ray crystallography, single crystals were attached with Paratone N to a fibre loop supported in a copper mounting pin, and then quenched in a cold nitrogen stream. Data were collected at 100 K using Cu-Kα radiation (micro-source, mirror monochromated) using an Agilent Supernova, Dual, Cu at zero diffractometer with an Atlas detector. Data processing was undertaken with CrysAlisPro.[50] A multiscan absorption correction was applied to the data. Structures were solved by direct methods with SHELXS-97, and extended and refined with SHELXL-97 using the X-Seed interface.[51,52] The non-hydrogen atoms in the asymmetric unit were modelled with anisotropic displacement parameters and a riding atom model with group displacement parameters used for the hydrogen atoms. X-ray crystallographic data is available in CIF format (supporting information). CCDC 1446715-1446719 contain the supplementary crystallographic data for this Article. These data can be obtained free of charge from The Cambridge Crystallographic Data Centre via www.ccdc.cam.ac.uk/data_request/cif.

Crystal data for 4-trimethylsilyl-2,6-dimethoxyphenylboronic acid: $C_{11}H_{19}BO_4Si$, M = 254.16, colourless block, 0.41 × 0.24 × 0.21 mm^3, monoclinic, a = 7.7685(12) Å, b = 12.973(2) Å, c = 13.791(2) Å, α = 90.00°, β = 103.162(9)°, γ = 90.00°, V = 1353.4(4) Å^3, space group P21/c (#14), Z = 4, μ(Mo Kα) = 0.173 mm–1, $2\theta_{max}$ = 56.52°, 25387 reflections measured, 3267 independent reflections (R_{int} = 0.0365). The final R_1(F) = 0.0384 (I > 2σ(I)); 0.0469 (all data). The final $wR_2(F^2)$ = 0.0965 (I > 2σ(I)); 0.1024 (all data). GoF = 1.048.

Crystal data for **BTD-NMe$_2$**: $C_{14}H_{13}N_3S$, *M* = 255.33, yellow needle, 0.23 × 0.08 × 0.04 mm^3, orthorhombic, *a* = 6.48560(10) Å, *b* = 16.0610(4) Å, *c* = 22.6793(6) Å, *α* = 90.00°, *β* = 90.00°, *γ* = 90.00°, *V* = 2362.39(9) Å^3, space group *Pbca* (#61), *Z* = 8, *μ*(Cu-K$_α$) = 2.288 mm^{-1}, $2\theta_{max}$ = 147.56°, 31297 reflections measured, 2349 independent reflections (R_{int} = 0.1128). The final $R_1(F)$ = 0.0791 ($I > 2\sigma(I)$); 0.0888 (all data). The final $wR_2(F^2)$ = 0.1247 ($I > 2\sigma(I)$); 0.1289 (all data). GoF = 1.082. CCDC 1446716

Crystal data for **BTD-TPA**: $C_{24}H_{17}N_3S$, *M* = 379.47, yellow plate, 0.44 × 0.22 × 0.02 mm^3, monoclinic, *a* = 19.4003(4) Å, *b* = 9.4082(2) Å, *c* = 21.1126(5) Å, *α* = 90.00°, *β* = 105.654(2)°, *γ* = 90.00°, *V* = 3710.58(14) Å^3, space group $P2_1/c$ (#14), *Z* = 8, *μ*(Cu-K$_α$) = 1.651 mm^{-1}, $2\theta_{max}$ = 153.42°, 23852 reflections measured, 7724 independent reflections (R_{int} = 0.0395). The final $R_1(F)$ = 0.0394 ($I > 2\sigma(I)$); 0.0459 (all data). The final $wR_2(F^2)$ = 0.1018 ($I > 2\sigma(I)$); 0.1080 (all data). GoF = 1.041. CCDC 1446717

Crystal data for **BTD-TPA$_2$**: $C_{42}H_{30}N_4S$, *M* = 622.76, orange hexagonal prism, 0.51 × 0.17 × 0.13 mm^3, orthorhombic, *a* = 6.8534(2) Å, *b* = 18.7576(4) Å, *c* = 24.5481(5) Å, *α* = 90.00°, *β* = 90.00°, *γ* = 90.00°, *V* = 3155.74(13) Å^3, space group *Pbcn*(#60), *Z* = 4, *μ*(Cu-K$_α$) = 2.288 mm^{-1}, $2\theta_{max}$ = 147.04°, 12262 reflections measured, 3122 independent reflections (R_{int} = 0.0304). The final $R_1(F)$ = 0.0449 ($I > 2\sigma(I)$); 0.0462 (all data). The final $wR_2(F^2)$ = 0.1252 ($I > 2\sigma(I)$); 0.1268 (all data). GoF = 1.043. CCDC 1446718

Crystal data for **BTD-(OMe)$_2$TPA**: $C_{26}H_{21}N_3O_2S$, *M* = 439.52, yellow needle, 0.62 × 0.11 × 0.03 mm^3, triclinic, *a* = 11.2770(5) Å, *b* = 11.7982(5) Å, *c* = 17.6321(4) Å, *α* = 93.230(3)°, *β* = 90.383(3)°, *γ* = 113.527(4)°, *V* = 2146.40(14) Å^3, space group *P*-1(#2), *Z* = 4, *μ*(Cu-K$_α$) = 2.288 mm^{-1}, $2\theta_{max}$ = 149.14°, 19921 reflections measured, 8458 independent reflections (R_{int} = 0.0336). The final $R_1(F)$ = 0.0408 ($I > 2\sigma(I)$); 0.0475 (all data). The final $wR_2(F^2)$ = 0.1073 ($I > 2\sigma(I)$); 0.1136 (all data). GoF = 1.029. CCDC1446719

FT-Raman spectra were recorded using a Bruker MultiRAM spectrometer implementing a 1064 nm excitation at 600 mW power, a resolution of 4 cm^{-1} and 500 co-added scans. Differential Raman cross sections were calculated using Origin Pro 7.5 peak integration on strong peaks at ~1176, ~1215, ~1295, ~1595 and ~1613 cm^{-1} which represent peaks 1 through 5 (respectively) used

for cross section analysis. Differential Raman cross-sections are obtained by comparison of the peak areas with reported differential Raman cross-sections of solvent as described in the literature.[53] In short, solute differential Raman cross-sections were obtained relative to solvent cross-sections using the following equation:

$$\left(\frac{d\sigma_R}{d\Omega}\right)_u = \frac{I_u}{I_v}\frac{C_v}{C_u}\left(\frac{d\sigma_R}{d\Omega}\right)_v \qquad Equation\ 1.$$

Where $(d\sigma_R/d\Omega)_u$ is the is the differential Raman cross-section of the solute band of interest, I_u and I_v are the fully corrected observed intensities for the solute and solvent, respectively, c_u and c_v are the concentrations of solute and solvent and $(d\sigma_R/d\Omega)_v$v is the differential Raman cross-section of a solvent band. Solvent Raman cross sections were retrieved from the literature including acetonitrile and toluene.[54,55]

Electronic absorption spectra were measured on 1×10^{-5} M solutions implementing an OceanOptics USB2000 spectrometer.

Emission spectra were recorded using the same setup as resonance Raman, with light instead dispersed in the horizontal plane by a 300 grooves mm^{-1} diffraction grating. Spectra were measured on 1×10^{-5} M solutions. Onsager radii used for Lippert Mataga analysis is taken as half the distance of the molecular long axis.

The electrochemical cell for cyclic voltammetry was made up of a 1 mm diameter platinum rod working electrode embedded in a KeL-F cylinder with a platinum auxiliary electrode and a Ag/AgCl reference electrode. The potential of the cell was controlled by an ADI Powerlab 4SP potentiostat. Solutions were typically about 10^{-3} M in CH_2Cl_2 with 0.1 M tetrabutylammonium hexafluorophosphate (n-Bu_4PF_6) as a supporting electrolyte, and were purged with argon for approximately 5 min prior to measurement. The scanning speed was 100 mV s^{-1}, and the cyclic voltammograms were calibrated against the decamethylferrocenium/decamethylferrocene (Fc^{*+}/Fc^{*}) couple (-0.012 V in CH_2Cl_2) and are reported relative to the saturated calomel electrode (SCE) for comparison with other data by subtracting 0.045 V.[56]

Materials

1-Trimethylsilyl-3,5-dimethoxybenzene

A solution of 1-bromo-3,5-dimethoxybenzene (3.18 g, 14.7 mmol) in anhydrous THF (30 mL) was cooled to -78 °C using a dry ice bath, and n-BuLi (11.0 mL, 2.0 M in hexane) added dropwise under an argon atmosphere. The reaction mixture was stirred at -78 °C for 2 h under an argon atmosphere. Me_3SiCl (4.5 mL, 35.5 mmol) was added dropwise and the reaction mixture stirred at rt for 15 h. The product was extracted into CH_2Cl_2 and washed with NH_4Cl solution (sat.), then water. The organic extract was dried over $MgSO_4$, and the solvent removed under reduced pressure. The residue was purified using preparative column chromatography (SiO_2, CH_2Cl_2) to afford 1-trimethylsilyl-3,5-dimethoxybenzene (3.00 g, 97%) as a colorless oil. ^{1}H NMR (400 MHz, $CDCl_3$):[57] δ 6.65 (d, J = 2.3 Hz, 2H, H_2), 6.46 (t, J = 2.3 Hz, 1H, H_4), 3.81 (s, 6H, O*Me*), 0.26 (s, 9H, SiMe_3) ppm.

4-Trimethylsilyl-2,6-dimethoxyphenylboronic acid

A solution of trimethylsilyl-3,5-dimethoxybenzene (2.87 g, 13.7 mmol) in anhydrous THF (20 mL) was cooled to 0 °C using an ice bath, and n-BuLi (11.0 mL, 2.0 M in hexane) added dropwise under an argon atmosphere. The reaction mixture was stirred at 0 °C for 15 h under an argon atmosphere. $B(OMe)_3$ (3.5 mL, 31.4 mmol) was added dropwise and the reaction mixture stirred at rt for 5 h. NH_4Cl solution (sat.) was then added and the reaction mixture stirred at rt for 2 h. The product was extracted into CH_2Cl_2 and washed with NH_4Cl solution (sat.), then water. The organic extract was dried over $MgSO_4$, and the solvent removed under reduced pressure. The product was recrystallized from hexane to afford 4-trimethylsilyl-2,6-dimethoxyphenylboronic acid (2.39 g, 69%) as a white crystalline solid. An alternative purification using preparative column chromatography (SiO_2, 1:3 ethyl acetate/hexane) affords the product in 63% yield. ^{1}H NMR (500 MHz, $CDCl_3$): δ 7.24 (s, 2H, $B(OH)_2$), 6.75 (s, 2H, H_3), 3.94 (s, 6H, O*Me*), 0.30 (s, 9H, SiMe_3) ppm. ^{13}C NMR (126 MHz, $CDCl_3$): δ 165.01 (C_2), 147.37 (C_4), 108.85 (C_3), 56.27 (O*Me*), -1.05 (SiMe_3) ppm.

5-(2,6-Dimethoxyphenyl)benzo[c][1,25]thiadiazole (**BTD-(OMe)$_2$Ph**)

A mixture of 5-bromobenzo[*c*][1,2,5]thiadiazole(0.541 g, 2.51 mmol), 2,6-dimethoxyphenylboronic acid (0.719 g, 2.95 mmol) and K_2CO_3 (2.41 g, 17.4 mmol) in toluene (20 mL), H_2O (10 mL) and EtOH (5 mL) was bubbled with argon for 15 min. $PdCl_2$(dppf) (0.212 g, 0.290 mmol) was added and the reaction mixture heated at reflux for 15 h under an argon atmosphere. The reaction mixture was allowed to cool, and the product extracted into $CHCl_3$, and washed with NH_4Cl solution (sat.), then water. The organic extract was dried over $MgSO_4$, and the solvent removed under reduced pressure. The residue was purified using preparative column chromatography (SiO_2, CH_2Cl_2) to afford **BTD-(OMe)$_2$Ph** (0.596 g, 87%) as a white solid. ^{1}H NMR (500 MHz, $CDCl_3$): δ 8.00 (s, 1H, H_4), 7.99 (d, J = 9.0 Hz, 1H, H_7), 7.60 (dd, J = 9.0, 1.4 Hz, 1H, H_6), 7.36 (t, J = 8.4 Hz, 1H, $H_{4'}$), 6.71 (d, J = 8.4 Hz, 2H, $H_{3'}$), 3.77 (s, 6H, O*Me*) ppm. ^{13}C NMR (126 MHz, $CDCl_3$): δ 157.70 ($C_{2'}$), 155.19 (C_{3a}), 154.19 (C_{7a}), 136.05 (C_5),

134.06 (C_6), 129.75 ($C_{4'}$), 123.14 (C_4), 119.98 (C_7), 117.83 ($C_{1'}$), 104.30 ($C_{3'}$), 56.00 (O*Me*) ppm. MS (MALDI-TOF) calcd for $C_{14}H_{12}N_2O_2S$ ($[M]^+$): *m/z* 272.06. Found: *m/z* 272.03. Elemental analysis calcd for $C_{14}H_{12}N_2O_2S$: C, 61.75; H, 4.44; N, 10.29. Found: C, 61.51; H, 4.72; N, 10.29.

5-(4-Dimethylaminophenyl)benzo[c][1,2,5]thiadiazole (**BTD-NMe$_2$**)

A mixture of 5-bromobenzo[*c*][1,2,5]thiadiazole (0.508 g, 2.36 mmol), 4-dimethylaminophenylboronic acid (0.539 g, 3.27 mmol) and K_2CO_3 (1.72 g, 12.4 mmol) in toluene (20 mL), water (10 mL) and EtOH (5 mL) was bubbled with argon for 15 min. $PdCl_2$(dppf) (0.112 g, 0.153 mmol) was added and the reaction mixture heated at reflux for 15 h under an argon atmosphere. The reaction mixture was allowed to cool to rt, and the product extracted into CH_2Cl_2, and washed with NH_4Cl solution (sat.), then water. The organic extract was dried over $MgSO_4$, and the solvent removed under reduced pressure. The residue was purified using preparative column chromatography (SiO_2, CH_2Cl_2) to afford **BTD-NMe$_2$** (0.453 g, 75%) as a yellow crystalline solid. ^{1}H NMR (500 MHz, $CDCl_3$): δ 8.09 (d, J = 1.7 Hz, 1H, H_4), 8.00 (d, J = 9.2 Hz, 1H, H_7), 7.90 (dd, J = 9.2, 1.8 Hz, 1H, H_6), 7.64 (d, J = 8.9 Hz, 2H, $H_{2'}$), 6.85 (d, J = 7.0 Hz, 2H, $H_{3'}$), 3.04 (s, 6H, N*Me*$_2$) ppm. ^{13}C NMR (126 MHz, $CDCl_3$): δ 155.96 (C_{3a}), 155.22 ($C_{1'}$), 154.05 (C_{7a}), 150.70 ($C_{4'}$), 142.56 (C_5), 130.24 (C_6), 128.35 ($C_{2'}$), 121.28 (C_7), 116.41 (C_4), 112.89 ($C_{3'}$), 40.62 (NMe_2) ppm. HRMS (ESI) calcd for $C_{14}H_{14}N_3S$ ($[M+H]^+$): *m/z* 256.090. Found: *m/z* 256.092. Elemental analysis calcd for $C_{14}H_{13}N_3S$: C, 65.86; H, 5.13; N, 16.46. Found: C, 66.10; H, 5.32; N, 16.52.

5-(4-Diphenylaminophenyl)benzo[c][1,2,5]thiadiazole (**BTD-TPA**)

A mixture of 5-bromobenzo[*c*][1,2,5]thiadiazole (0.516 g, 2.40 mmol), 4-diphenylaminophenylboronic acid (0.890 g, 3.08 mmol) and K_2CO_3 (1.84 g, 13.3 mmol) in toluene (15 mL), H_2O (10 mL) and EtOH (5 mL) was bubbled with argon for 15 min. $PdCl_2$(dppf) (0.100 g, 0.122 mmol) was added and the reaction mixture heated at reflux for 15 h under an argon atmosphere. The reaction mixture was allowed to cool, and the product extracted into $CHCl_3$, and washed with NH_4Cl solution (sat.), then water. The organic extract was dried over $MgSO_4$, and the solvent removed under reduced pressure. The residue was purified using preparative column chromatography (SiO_2, CH_2Cl_2) to afford **BTD-TPA** (0.856 g, 94%) as a yellow crystalline solid. ^{1}H NMR (500 MHz, $CDCl_3$): δ 8.13 (dd, J = 1.7, 0.7 Hz, 1H, H_4), 8.03 (dd, J = 9.2, 0.7 Hz, 1H, H_7), 7.89 (dd, J = 9.2, 1.8 Hz, 1H, H_6), 7.59 (d, J = 8.7 Hz, 2H, $H_{2'}$), 7.30 (dd, J = 8.5, 7.4 Hz, 4H, $H_{3''}$), 7.18 (d, J = 8.7 Hz, 2H, $H_{3'}$), 7.17 (dd, J = 8.5, 1.0 Hz, 4H, $H_{2''}$), 7.08 (tt, J = 7.4, 1.1 Hz, 2H, $H_{4''}$) ppm. ^{13}C NMR (126 MHz, $CDCl_3$): δ 155.72 (C_{3a}), 154.20 (C_{7a}), 148.47 ($C_{4'}$), 147.49 ($C_{1''}$), 142.05 (C_5), 132.79 ($C_{1'}$), 130.10 (C_6), 129.55 ($C_{3''}$), 128.29 ($C_{2'}$), 125.02 ($C_{2''}$), 123.60 ($C_{4''}$), 123.35 ($C_{3'}$), 121.49 (C_7), 117.50 (C_4) ppm. HRMS (ESI) calcd for $C_{24}H_{18}N_3S$ ($[M+H]^+$): *m/z* 380.122. Found: *m/z* 380.121. Elemental analysis calcd for $C_{24}H_{17}N_3S$: C, 75.69; H, 4.52; N, 11.07. Found: C, 75.66; H, 4.37; N, 11.02.

5,6-Di(4-diphenylaminophenyl)benzo[c][1,2,5]thiadiazole (**BTD-TPA$_2$**)

A mixture of 5,6-dibromobenzo[*c*][1,2,5]thiadiazole (0.132 g, 0.449 mmol), 4-diphenylaminophenylboronic acid (0.420 g, 1.45 mmol) and K_2CO_3 (0.500 g, 3.62 mmol) in toluene (20 mL), H_2O (10 mL) and EtOH (5 mL) was bubbled with argon for 15 min. $PdCl_2$(dppf) (0.062 g, 0.076 mmol) was added and the reaction mixture heated at reflux for 15 h under an argon atmosphere. The reaction mixture was allowed to cool, and the product extracted into $CHCl_3$, and washed with NH_4Cl solution (sat.), then water. The organic extract was dried over $MgSO_4$, and the solvent removed under reduced pressure. The residue was purified using preparative column chromatography (SiO_2, CH_2Cl_2) to afford **BTD-TPA$_2$** (0.203 g, 72%) as a yellow solid. ^{1}H NMR (500 MHz, $CDCl_3$): δ 8.02 (s, 2H, $H_{4,7}$), 7.26 (t, J = 7.3 Hz, 8H, $H_{3''}$), 7.11 (dd, J = 8.5, 1.1 Hz, 8H, $H_{2''}$), 7.06 (d, J = 8.7 Hz, 4H, $H_{2'}$), 7.04 (t, J = 7.3 Hz, 4H, $H_{4''}$), 6.99 (d, J = 8.6 Hz, 4H, $H_{3'}$) ppm. ^{13}C NMR (126 MHz, $CDCl_3$): δ 154.55 ($C_{3a,7a}$), 147.66 ($C_{1''}$), 147.32 ($C_{4'}$), 143.84 ($C_{5,6}$), 134.22 ($C_{1'}$), 130.80 ($C_{2'}$), 129.49 ($C_{3''}$), 124.75 ($C_{2''}$), 123.29 ($C_{4''}$), 122.68 ($C_{3'}$), 121.29 ($C_{4,7}$) ppm. MS (MALDI-TOF) calcd for $C_{42}H_{30}N_4S$ ($[M]^+$): *m/z* 622.22. Found: *m/z* 622.21. Elemental analysis calcd for $C_{42}H_{30}N_4S$: C, 81.00; H, 4.86; N, 9.00. Found: C, 81.28; H, 5.06; N, 8.87.

5-(4-Trimethylsilyl-2,6-dimethoxyphenyl)benzo[c][1,2,5]thiadiazole

A mixture of 5-bromobenzo[*c*][1,2,5]thiadiazole (0.358 g, 1.67 mmol), 4-trimethylsilyl-2,6-dimethoxyphenylboronic acid (0.510 g, 2.01 mmol) and K_2CO_3 (1.22 g, 8.82 mmol) in toluene (20 mL), H_2O (10 mL) and EtOH (5 mL) was bubbled with argon for 15 min. $PdCl_2$(dppf) (0.130 g, 0.159 mmol) was added and the reaction mixture heated at reflux for 15 h under an argon atmosphere. The reaction mixture was allowed to cool, and the product extracted into $CHCl_3$, and washed with NH_4Cl solution (sat.), then water. The organic extract was dried over $MgSO_4$, and the solvent removed under reduced pressure. The residue was purified using preparative column chromatography (SiO_2, CH_2Cl_2) to afford 5-(4-trimethylsilyl-2,6-

dimethoxyphenyl)benzo[*c*][1,2,5]thiadiazole (0.549 g, 96%) as a white solid. ^{1}H NMR (500 MHz, $CDCl_3$): δ 8.00 (dd, J = 1.5, 0.8 Hz, 1H, H_4), 7.98 (dd, J = 9.0, 0.8 Hz, 1H, H_7), 7.61 (dd, J = 9.0, 1.6 Hz, 1H, H_6), 6.84 (s, 2H, $H_{3'}$), 3.80 (s, 6H, O*Me*), 0.36 (s, 9H, Si*Me*$_3$) ppm. ^{13}C NMR (126 MHz, $CDCl_3$): δ 157.12 ($C_{2'}$), 155.20 (C_{3a}), 154.22 (C_{7a}), 142.95 ($C_{4'}$), 136.12 (C_5), 134.03 (C_6), 123.14 (C_4), 119.97 (C_7), 118.57 ($C_{1'}$), 108.74 ($C_{3'}$), 56.05 (O*Me*), 0.92 (Si*Me*$_3$) ppm. MS (MALDI-TOF) calcd for $C_{17}H_{20}N_2O_2SSi$ ($[M]^+$): *m/z* 344.10. Found: *m/z* 344.08. Elemental analysis calcd for $C_{17}H_{20}N_2O_2SSi$: C, 59.27; H, 5.85; N, 8.13. Found: C, 59.10; H, 5.92; N, 8.02.

5-(4-Iodo-2,6-dimethoxyphenyl)benzo[c][1,2,5]thiadiazole

A solution of 5-(4-trimethylsilyl-2,6-dimethoxyphenyl)benzo[*c*][1,2,5]thiadiazole (0.549 g, 1.59 mmol) in CH_2Cl_2 (100 mL) was cooled to -78 °C using a dry ice/acetone bath under an argon atmosphere. ICl (2.5 mL, 1 M in CH_2Cl_2) was added dropwise and the resultant mixture stirred at -78 °C under an argon atmosphere for 2 h. The dry ice/acetone bath was removed, excess ICl quenched by dropwise addition of aqueous $Na_2S_2O_4$ (sat., 20 mL), and the mixture allowed to warm to rt. The product was extracted into CH_2Cl_2 and washed with aqueous NH_4Cl (sat.), then water. The organic extract was dried over $MgSO_4$, and the solvent removed under reduced pressure. The residue was purified using preparative column chromatography (SiO_2, CH_2Cl_2) to afford 5-(4-Iodo-2,6-dimethoxyphenyl)benzo[*c*][1,2,5]thiadiazole (0.505 g, 80%) as a white solid. ^{1}H NMR (500 MHz, $CDCl_3$): δ 7.97 (d, J = 9.1 Hz, 1H, H_7), 7.94 (s, 1H, H_4), 7.53 (d, J = 9.0, 1.4 Hz, 1H, H_6), 7.03 (s, 2H, $H_{3'}$), 3.75 (s, 6H, O*Me*) ppm. ^{13}C NMR (126 MHz, $CDCl_3$): δ 157.92 ($C_{2'}$), 155.07 (C_{3a}), 154.22 (C_{7a}), 135.13 (C_5), 133.58 (C_6), 123.16 (C_4), 120.17 (C_7), 117.81 ($C_{1'}$), 114.23 ($C_{3'}$), 93.92 ($C_{4'}$), 56.30 (O*Me*) ppm. MS (MALDI-TOF) calcd for $C_{14}H_{11}IN_2O_2S$ ($[M]^+$): *m/z* 397.96. Found: *m/z* 397.92. Elemental analysis calcd for $C_{14}H_{11}IN_2O_2S$: C, 42.23; H, 2.78; N, 7.03. Found: C, 42.35; H, 2.76; N, 7.11.

5-(4-Diphenylamino-2,6-dimethoxyphenyl)benzo[c][1,2,5]thiadiazole (**BTD-(OMe)$_2$TPA**)

A mixture of 5-(4-iodo-2,6-dimethoxyphenyl)benzo[*c*][1,2,5]thiadiazole (0.292 g, 0.733 mmol), diphenylamine (0.229 g, 1.35 mmol) and *t*-BuOK (0.264 g, 2.35 mmol) in toluene (20 mL) was bubbled with argon for 15 min. [*t*-Bu$_3$PH]BF_4 (0.032 g, 0.112 mmol) and $Pd_2(dba)_3$ (0.060 g, 0.065 mmol) were added and the reaction mixture heated at reflux for 15 h under an argon atmosphere. The reaction mixture was allowed to cool to rt, and the product extracted into $CHCl_3$, and washed with NH_4Cl solution (sat.), then water. The organic extract was dried over $MgSO_4$, and the solvent removed under reduced pressure. The residue was purified using preparative column chromatography (SiO_2, CH_2Cl_2) to afford **BTD-(OMe)$_2$TPA** (0.367 g, 50%) as a yellow crystalline solid. ^{1}H NMR (500 MHz, $CDCl_3$): δ 8.02 (dd, J = 1.4, 0.7 Hz, 1H, H_4), 7.96 (dd, J = 9.1, 0.7 Hz, 1H, H_7), 7.64 (dd, J = 9.1, 1.5 Hz, 1H, H_6), 7.31 (dd, J = 8.4, 7.4 Hz, 4H, $H_{3''}$), 7.21 (dd, J = 8.6, 1.0 Hz, 4H, $H_{2''}$), 7.08 (tt, J = 7.3, 1.0 Hz, 2H, $H_{4''}$), 6.38 (s, 2H, $H_{3'}$), 3.58 (O*Me*) ppm. ^{13}C NMR (126 MHz, $CDCl_3$): δ 158.15 ($C_{2'}$), 155.30 (C_{3a}), 154.11 (C_{7a}), 149.55 ($C_{4'}$), 147.51 ($C_{1''}$), 136.07 (C_5), 134.48 (C_6), 129.43 ($C_{3''}$), 125.04 ($C_{2''}$), 123.51 ($C_{4''}$), 123.18 (C_4), 119.76 (C_7), 112.11 ($C_{1'}$), 99.87 ($C_{3'}$), 55.97 (O*Me*) ppm. HRMS (ESI) calcd for $C_{26}H_{22}N_3O_2S$ ($[M+H]^+$): *m/z* 440.143. Found: *m/z* 440.143. Elemental analysis calcd for $C_{26}H_{21}N_3O_2S$: C, 71.05; H, 4.82; N, 9.56. Found: C, 71.05; H, 4.86; N, 9.62.

4-Methyl-1,2-di(tosylamino)benzene

A mixture of 4-methyl-1,2-phenylenediamine (8.01 g, 65.5 mmol) and pyridine (20 mL, 250 mmol) in CH_2Cl_2 (150 mL) was cooled to 0 °C using an ice bath. TsCl (30.0 g, 157 mmol) was added in small portions, the reaction mixture warmed to rt, and stirred for 3 h at rt. The product was extracted into CH_2Cl_2, and washed with NH_4Cl solution (sat.), then water. The organic extract was dried over $MgSO_4$, and the solvent removed under reduced pressure. The residue was recrystallised from EtOH to afford 4-methyl-1,2-di(tosylamino)benzene (26.8 g, 95%) as a white solid. ^{1}H NMR (500 MHz, $CDCl_3$): δ 7.60 (d, J = 8.3 Hz, 2H, $H_{2'/2''}$), 7.53 (d, J = 8.3 Hz, 2H, $H_{2'/2''}$), 7.22 (dd, J = 8.6, 0.6 Hz, 2H, $H_{3'/3''}$), 7.21 (dd, J = 8.6, 0.6 Hz, 2H, $H_{3'/3''}$), 7.02 (s, 1H, N*H*), 6.93 (d, J = 1.4 Hz, 1H, H_3), 6.79 (ddd, J = 8.1, 2.0, 0.7 Hz, 1H, H_5), 6.67 (d, J = 8.1 Hz, 1H, H_6), 6.43 (s, 1H, N*H*), 2.39 (s, 6H, Ts-*Me*), 2.19 (s, 3H, *Me*) ppm. ^{13}C NMR (126 MHz, $CDCl_3$): δ 144.31 ($C_{4'/4''}$), 144.16 ($C_{4'/4''}$), 138.45 (C_4), 135.97 ($C_{1'/1''}$), 135.44 ($C_{1'/1''}$), 131.97 (C_2), 129.75 ($C_{3'/3''}$), 129.69 ($C_{3'/3''}$), 127.80 (C_5), 127.70 ($C_{2'/2''}$), 127.64 ($C_{2'/2''}$), 127.20 (C_1), 127.08 (C_6), 126.41 (C_3), 21.75 (Ts-*Me*), 21.73 (Ts-*Me*), 21.16 (*Me*) ppm. HRMS (ESI) calcd for $C_{21}H_{22}N_2NaO_4S_2$ ($[M+Na]^+$): *m/z* 453.091. Found: *m/z* 453.093. Elemental analysis calcd for $C_{21}H_{22}N_2O_4S_2$: C, 58.58; H, 5.15; N, 6.51. Found: C, 58.48; H, 5.14; N, 6.66.

4-Bromo-5-methyl-1,2-di(tosylamino)benzene

A mixture of 4-methyl-1,2-di(tosylamino)benzene (23.0 g) and AcONa (8.00 g, 98.0 mmol) in AcOH (200 mL) was cooled to 0 °C using an ice bath. Br_2 (3.5 mL, 68.0 mmol) was added dropwise, and the reaction mixture heated at reflux for 3 h. Water was added, and the precipitate filtered and washed with water. The residue was recrystallised from EtOH to afford 4-bromo-5-methyl-1,2-

di(tosylamino)benzene (24.8 g, 91%) as a white solid. ^{1}H NMR (500 MHz, $CDCl_3$): δ 7.59 (d, J = 8.3 Hz, 2H, $H_{2'/2''}$), 7.56 (d, J = 8.3 Hz, 2H, $H_{2'/2''}$), 7.26 (d, J = 7.8 Hz, 2H, $H_{3'/3''}$), 7.25 (d, J = 7.9 Hz, 2H, $H_{3'/3''}$), 7.01 (s, 1H, H_3), 6.93 (s, 1H, H_6), 6.91 (s, 1H, N*H*), 6.56 (s, 1H, N*H*), 2.41 (s, 3H, Ts-*Me*), 2.40 (s, 3H, Ts-*Me*), 2.21 (s, 3H, *Me*) ppm. ^{13}C NMR (126 MHz, $CDCl_3$): δ 144.69 ($C_{4'/4''}$), 144.49 ($C_{4'/4''}$), 137.95 (C_5), 135.62 ($C_{1'/1''}$), 135.16 ($C_{1'/1''}$), 130.69 (C_1), 130.11 (C_3), 129.90 ($C_{3'/3''}$), 129.84 ($C_{3'/3''}$), 128.98 (C_2), 127.69 ($C_{2'/2''}$), 126.67 (C_6), 126.64 ($C_{2'/2''}$), 122.30 (C_4), 22.66 (*Me*), 21.77 (Ts-*Me*), 21.76 (Ts-*Me*) ppm. HRMS (ESI) calcd for $C_{21}H_{21}BrN_2NaO_4S_2$ ([M+Na]$^+$): *m/z* 531.002. Found: *m/z* 530.999. Elemental analysis calcd for $C_{21}H_{21}BrN_2O_4S_2$: C, 49.51; H, 4.15; N, 5.50. Found: C, 49.62; H, 4.01; N, 5.57.

4-Bromo-5-methyl-1,2-phenylenediamine

A mixture of 4-bromo-5-methyl-1,2-di(tosylamino)benzene (4.14 g, 8.13 mmol) and conc. H_2SO_4 (12 mL) was heated at reflux for 3 h. The reaction mixture was cooled to 0 °C, and water added. Aqueous NaOH (2 M) was added dropwise to achieve pH 5. The product was extracted into $CHCl_3$ to afford 4-bromo-5-methyl-1,2-phenylenediamine (1.42 g, 87%) as an off-white solid. ^{1}H NMR (500 MHz, $(CD_3)_2SO$): δ 6.66 (s, 1H, H_3), 6.43 (s, 1H, H_6), 4.51 (s, 4H, NH_2), 2.08 (s, 3H, *Me*) ppm. ^{13}C NMR (126 MHz, $(CD_3)_2SO$): δ 134.77 (C_1), 134.69 (C_2), 124.04 (C_5), 116.90 (C_3), 116.24 (C_6), 109.90 (C_4), 21.32 (*Me*) ppm. HRMS (ESI) calcd for $C_7H_{10}BrN_2$ ([M+H]$^+$): *m/z* 201.002. Found: *m/z* 201.002. Elemental analysis calcd for $C_7H_9BrN_2 \cdot H_2O$: C, 38.38; H, 5.06; N, 12.79. Found: C, 38.49; H, 4.98; N, 12.82.

5-Bromo-6-methylbenzo[c][1,2,5]thiadiazole

Thionyl chloride (0.8 mL, 11.0 mmol) was added dropwise to a mixture of 4-bromo-5-methyl-1,2-phenylenediamine (1.02 g, 5.08 mmol) and NEt_3 (5 mL, 35.9 mmol) in CH_2Cl_2 (50 mL). The reaction mixture was heated at reflux for 15 h, then allowed to cool to rt. HCl (100 mL, 5 M) was added and the reaction mixture stirred for 1 h. The product was extracted into CH_2Cl_2 and washed with NH_4Cl solution (sat.), then water. The organic extract was dried over $MgSO_4$, and the solvent removed under reduced pressure. The residue was purified using flash chromatography (SiO_2, CH_2Cl_2) to afford **BTDMe-Br** (1.05 g, 90%) as an off-white solid. ^{1}H NMR (500 MHz, $CDCl_3$): δ 8.25 (s, 1H, H_4), 7.83 (s, 1H, H_7), 2.58 (s, 3H, *Me*) ppm. ^{13}C NMR (126 MHz, $CDCl_3$): δ 154.13 (C_{7a}), 154.02 (C_{3a}), 139.69 (C_6), 128.95 (C_5), 124.08 (C_4), 120.70 (C_7), 24.09 (*Me*) ppm. MS (MALDI-TOF) calcd for $C_7H_5BrN_2S$ ([M]$^+$): *m/z* 227.94. Found: *m/z* 227.92. Elemental analysis calcd for $C_7H_5BrN_2S$: C, 36.70; H, 2.20; N, 12.23. Found: C, 36.51; H, 1.86; N, 11.93.

5-(4-Diphenylaminophenyl)-6-methylbenzo[c][1,2,5]thiadiazole (**BTDMe-TPA**)

A mixture of 5-bromo-6-methylbenzo[c][1,2,5]thiadiazole (0.532 g, 2.32 mmol), 4-diphenylaminophenylboronic acid (0.928 g, 3.21 mmol) and K_2CO_3 (1.71 g, 12.4 mmol) in toluene (20 mL), H_2O (10 mL) and EtOH (5 mL) was bubbled with argon for 15 min. $PdCl_2$(dppf) (0.131 g, 0.179 mmol) was added and the reaction mixture heated at reflux for 15 h under an argon atmosphere. The reaction mixture was allowed to cool, and the product extracted into $CHCl_3$, and washed with NH_4Cl solution (sat.), then water. The organic extract was dried over $MgSO_4$, and the solvent removed under reduced pressure. The residue was purified using preparative column chromatography (SiO_2, CH_2Cl_2) to afford **BTDMe-TPA** (0.735 g, 80%) as a yellow solid. ^{1}H NMR (500 MHz, $CDCl_3$): δ 7.86 (s, 1H, H_7), 7.85 (s, 1H, H_4), 7.30 (t, J = 7.5 Hz, 4H, $H_{3''}$), 7.24 (d, J = 8.5 Hz, 2H, $H_{2'}$), 7.18 (d, J = 7.7 Hz, 4H, $H_{2''}$), 7.15 (d, J = 8.5 Hz, 2H, $H_{3'}$), 7.07 (t, J = 7.3 Hz, 2H, $H_{4''}$), 2.45 (s, 3H, *Me*) ppm. ^{13}C NMR (126 MHz, $CDCl_3$): δ 154.57 (C_{7a}), 154.11 (C_{3a}), 147.66 ($C_{1''}$), 147.62 ($C_{4'}$), 145.22 (C_5), 139.53 (C_6), 134.03 ($C_{1'}$), 129.92 ($C_{2'}$), 129.49 ($C_{3''}$), 124.87 ($C_{2''}$), 123.37 ($C_{4''}$), 122.80 ($C_{3'}$), 120.83 (C_4), 120.75 (C_7), 22.19 (*Me*) ppm. MS (MALDI-TOF) calcd for $C_{25}H_{20}N_3S$ ([M+H]$^+$): *m/z* 393.14. Found: *m/z* 393.12. Elemental analysis calcd for $C_{25}H_{19}N_3S$: C, 76.31; H, 4.87; N, 10.68. Found: C, 76.71; H, 5.09; N, 10.59.

5-Azidobenzo[c][1,2,5]thiadiazole

A mixture of 5-aminobenzo[*c*][1,2,5]thiadiazole (1.50 g, 9.89 mmol) and TsOH (6.34 g, 33.3 mmol) in CH_3CN (100 mL) was cooled to 0 °C using an ice bath. A solution of $NaNO_2$ (1.78 g, 25.8 mmol) in water (10 mL) was added dropwise, and the reaction mixture stirred at 0 °C for 30 min. A solution of NaN_3 (3.30 g, 50.8 mmol) in water (10 mL) was added dropwise, and the reaction mixture stirred at rt for 2 h. Aq. $Na_2S_2O_3$ (sat.) was added, and the product extracted into EtOAc. The organic extract was dried over $MgSO_4$, and the solvent removed under reduced pressure. The residue was purified using flash chromatography (SiO_2, CH_2Cl_2) to afford 5-azobenzo[*c*][1,2,5]thiadiazole (0.353 g, 20%) as an off-white solid. The product was reacted without further characterisation. ^{1}H NMR (400 MHz, $CDCl_3$): δ 7.97 (d, J = 9.3 Hz, 1H, H_7), 7.64 (d, J = 2.2 Hz, 1H, H_4), 7.27 (dd, J = 9.3, 2.2 Hz, 1H, H_6) ppm.

5-(4-(4-Diphenylaminophenyl)-1,2,3-triazol-1-yl)-benzo[c][1,2,5]thiadiazole (**BTD-TRZTPA**)

A mixture of 5-azidobenzo[*c*][1,2,5]thiadiazole (0.353 g, 1.99 mmol), 4-ethynyl-*N*,*N*-diphenylaniline (0.487 g, 1.81 mmol), L-ascorbic acid (0.453 g, 2.57 mmol), Na_2CO_3 (0.297 g, 2.80 mmol) and

$CuSO_4 \cdot 5H_2O$ (0.253 g, 1.01 mmol) in DMF (20 mL) and water (5 mL) was stirred at rt for 15 h. Aq. EDTA (0.1 M) and NH_4OH (0.1 M) was added, and the resulting precipitate filtered. The residue was purified using preparative column chromatography (SiO_2, 20% EtOAc in $CHCl_3$) to afford **BTD-TRZ-DPAB** (0.735 g, 91%) as a yellow solid. ^{1}H NMR (500 MHz, $CDCl_3$): δ 8.33 (dd, J = 1.8, 0.4 Hz, 1H, H_4), 8.31 (dd, J = 9.3, 2.1 Hz, 1H, H_6), 8.27 (s, 1H, $H_{5'}$), 8.20 (dd, J = 9.3, 0.4 Hz, 1H, H_7), 7.80 (d, J = 8.6 Hz, 2H, $H_{2''}$), 7.29 (dd, J = 8.2, 7.5 Hz, 4H, $H_{3''}$), 7.17 (d, J = 8.7 Hz, 2H, $H_{3''}$), 7.15 (d, J = 8.5 Hz, 4H, $H_{2''}$), 7.07 (tt, J = 7.4, 0.8 Hz, 2H, $H_{4''}$) ppm. ^{13}C NMR (126 MHz, $CDCl_3$): δ 154.53 (C_{3a}), 154.11 (C_{7a}), 149.10 ($C_{4'}$), 148.59 ($C_{4''}$), 147.55 ($C_{1''}$), 137.95 (C_5), 129.53 ($C_{3''}$), 127.01 ($C_{2''}$), 124.92 ($C_{2''}$), 123.62 (C_6), 123.50 ($C_{4''',1''}$), 123.49 ($C_{3''}$), 123.22 (C_7), 116.81 ($C_{5'}$), 110.85 (C_4) ppm. HRMS (ESI) calcd for $C_{26}H_{19}N_6S$ ($[M+H]^+$): m/z 447.139. Found: 447.137. Elemental analysis calcd for $C_{26}H_{18}N_6S$: C, 69.94; H, 4.06; N, 18.82. Found: C, 69.80; H, 4.12; N, 18.84.

ASSOCIATED CONTENT

Supporting Information. Electrochemical data; mean absolute deviations between FT and calculated Raman spectra in toluene and *vacuo*; experimental Raman spectra in acetonitrile, toluene and *vacuo*; experimental Raman cross-sections; electronic absorption data; calculated electronic absorption data; calculated molecular orbital energies (HOMOs and LUMOs); resonance Raman data collected with 351 nm excitation; calculated molecular orbital representations (HOMOs and LUMOs); emission data; Lippert-Mataga plots; scores plot for principle component 2 from principle component analysis; Hartree-Fock distance relationship plot for functionals used in this study; compound numbering scheme used for NMR assignments; crystallographic data in CIF format. This material is available free of charge via the Internet at http://pubs.acs.org.

AUTHOR INFORMATION

Corresponding Author

Correspondence should be addressed to Keith Gordon (kgordon@chemistry.otago.ac.nz) and Nigel T. Lucas (nlucas@chemistry.otago.ac.nz); fax: +64 3 479 7906, phone: +64 3 479 7908.

Author Contributions

‡These authors contributed equally.

Funding Sources

MacDiarmid Institute for Advanced Materials and Nanotechnology.

Notes

Authors declare no competing financial interest.

ACKNOWLEDGMENT

Support from the University of Otago and MacDiarmid Institute for Advanced Materials and Nanotechnology is gratefully acknowledged. Greg S. Huff from the University of Otago is recognized for an intellectual contribution towards this publication.

ABBREVIATIONS

DFT, Density Functional Theory; DA, Donor-Acceptor; CT, Charge Transfer; LDA, Local Density Approximations; GGA, Generalized Gradient Approximations; B3LYP, Becke, three-parameter, Lee-Yang-Parr; HF Hartree Fock; BTD, benzo[c][1,2,5]thiadiazole; MAD, Mean Absolute Deviation; HOMO, Highest Occupied Molecular Orbital; LUMO, Lowest Unoccupied Molecular Orbital; FMO, Frontier Molecular Orbital; TPA, Triphenylamine; MPE, Mean Percentage Error; PCA, Principal Component Analysis; PC, Principal Component.

REFERENCES

(1) Kippelen, B.; Brédas, J. L., Organic Photovoltaics, *Energy Environ. Sci.,* **2009**, *2*, 251-261.

(2) Hains, A. W.; Liang, Z.; Woodhouse, M. A.; Gregg, B. A., Molecular Semiconductors in Organic Photovoltaic Cells, *Chem. Rev.,* **2010**, *110*, 6689-6735.

(3) Facchetti, A., π-Conjugated Polymers for Organic Electronics and Photovoltaic Cell Applications, *Chem. Mater.,* **2011**, *23*, 733-758.

(4) Grossiord, N.; Kroon, J. M.; Andriessen, R.; Blom, P. W. M., Degradation Mechanisms in Organic Photovoltaic Devices, *Org. Electron.,* **2012**, *13*, 432-456.

(5) Neto, B. a. D.; Lapis, A. M.; Da Silva Júnior, E. N.; Dupont, J., 2,1,3-Benzothiadiazole and Derivatives: Synthesis, Properties, Reactions, and Applications in Light Technology of Small Molecules, *Eur. J. Org. Chem.,* **2013**, 228-255.

(6) Wu, Y.; Zhu, W., Organic Sensitizers From D-π-A to D-A-π-A: Effect of the Internal Electron-Withdrawing Units on Molecular Absorption, Energy Levels and Photovoltaic Performances, *Chem. Soc. Rev.,* **2013**, *42*, 2039-2058.

(7) Castellano, F. N., Altering Molecular Photophysics by Merging Organic and Inorganic Chromophores, *Acc. Chem. Res.,* **2015**, *48*, 828-839.

(8) Mishra, A.; Fischer, M. K. R.; Bäuerle, P., Metal-Free Organic Dyes for Dye-Sensitized Solar Cells: From Structure: Property Relationships to Design Rules, *Angew. Chem., Int. Ed.,* **2009**, *48*, 2474-2499.

(9) Lakowicz, J. R. *Principles of Fluorescence Spectroscopy*; Springer US, 2007.

(10) Laurent, A. D.; Jacquemin, D., TD-DFT Benchmarks: A Review, *Int. J. Quantum Chem.,* **2013**, *113*, 2019-2039.

(11) Casanova, D.; Rotzinger, F. P.; Grätzel, M., Computational Study of Promising Organic Dyes for High-Performance Sensitized Solar Cells, *J. Chem. Theory Comput.,* **2010**, *6*, 1219-1227.

(12) Wodrich, M. D.; Corminboeuf, C.; Schreiner, P. R.; Fokin, A. A.; Schleyer, P. v. R., How Accurate Are DFT Treatments of Organic Energy?, *Org. Lett.,* **2007**, *9*, 1851-1854.

(13) Pastore, M.; Mosconi, E.; De Angelis, F.; Grätzel, M., A Computational Investigation of Organic Dyes for Dye-Sensitized Solar Cells: Benchmark, Strategies, and Open Issues, *J. Phys. Chem. A,* **2010**, *114*, 7205-7212.

(14) Burke, K., Perspective on Density Functional Theory, *J. Chem. Phys.,* **2012**, *136*, 150901.

(15) Sousa, S. F.; Fernandes, P. A.; Ramos, M. J., General Performance of Density Functionals, *J. Phys. Chem. A,* **2007**, *111*, 10439-10452.

(16) Jacquemin, D.; Perpète, E. A.; Scuseria, G. E.; Ciofini, I.; Adamo, C., TD-DFT Performance for the Visible Absorption Spectra of Organic Dyes: Conventional Versus Long-Range Hybrids, *J. Chem. Theory Comput.,* **2008**, *4*, 123-135.

(17) Zheng, S. H.; Geva, E.; Dunietz, B. D., Solvated Charge Transfer States of Functionalized Anthracene and Tetracyanoethylene Dimers: A Computational Study Based on a Range Separated Hybrid Functional and Charge Constrained Self-Consistent Field with Switching Gaussian Polarized Continuum Models, *J. Chem. Theory Comput.,* **2013**, *9*, 1125-1131.

(18) Zhang, J.; Kan, Y. H.; Li, H. B.; Geng, Y.; Wu, Y.; Su, Z. M., How to Design Proper pi-Spacer Order of he D-pi-A Dyes for DSSCs? A Density Functional Response, *Dyes Pigm.,* **2012**, *95*, 313-321.

(19) Vijayakumar, T.; Joe, I. H.; Nair, C. P. R.; Jayakumar, V. S., Efficient pi Electrons Delocalization in Prospective Push-Pull Non-Linear Optical Chromophore 4- NN-dimethylamino -4 '-nitro stilbene (DANS): A Vibrational Spectroscopic Study, *Chem. Phys.,* **2008**, *343*, 83-99.

(20) Sarkar, A.; Das, M.; Bagchi, S., Electronic Spectra and Hyperpolarizabilities of Structurally Similar Donor–Acceptor Dyes. A Density Functional Theory Analysis, *J. Mol. Struct.,* **2015**, *1102*, 11-17.

(21) Pastore, M.; Fantacci, S.; De Angelis, F., Modeling Excited States and Alignment of Energy Levels in Dye-Sensitized Solar Cells: Successes, Failures, and Challenges, *J Phys. Chem C,* **2013**, *117*, 3685-3700.

(22) McCormick, T. M.; Bridges, C. R.; Carrera, E. I.; Di Carmine, P. M.; Gibson, G. L.; Hollinger, J.; Kozycz, L. M.; Seferos, D. S., Conjugated Polymers: Evaluating DFT Methods for More Accurate Orbital Energy Modeling, *Macromolecules,* **2013**, *46*, 3879-3886.

(23) Jamorski, C.; Foresman, J. B.; Thilgen, C.; Luthi, H. P., Assessment of Time-Dependent Density-Functional Theory for the Calculation of Critical Features in the Absorption Spectra of a Series of Aromatic Donor-Acceptor Systems, *J. Chem. Phys.,* **2002**, *116*, 8761-8771.

(24) Gierschner, J.; Cornil, J.; Egelhaaf, H. J., Optical Bandgaps of pi-Conjugated Organic Materials at the Polymer Limit: Experiment and Theory, *Adv. Mater.,* **2007**, *19*, 173-191.

(25) Champagne, B.; Perpete, E. A.; Jacquemin, D.; van Gisbergen, S. J. A.; Baerends, E. J.; Soubra-Ghaoui, C.; Robins, K. A.; Kirtman, B., Assessment of Conventional Density Functional Schemes for Computing the Dipole Moment and (Hyper)Polarizabilities of Push-Pull pi-Conjugated Systems, *J. Phys. Chem. A,* **2000**, *104*, 4755-4763.

(26) Andreu, R.; Blesa, M. J.; Carrasquer, L.; Garin, J.; Orduna, J.; Villacampa, B.; Alcala, R.; Casado, J.; Delgado, M. C. R.; Navarrete, J. T. L.; Allain, M., Tuning First Molecular Hyperpolarizabilities Through the Use of Proaromatic Spacers, *J. Am. Chem. Soc.,* **2005**, *127*, 8835-8845.

(27) Jacquemin, D.; Planchat, A.; Adamo, C.; Mennucci, B., TD-DFT Assessment of Functionals for Optical 0-0 Transitions in Solvated Dyes, *J. Chem. Theory Comput.,* **2012**, *8*, 2359-2373.

(28) Uno, T.; Ohta, H.; Yamane, A.; Kubo, M.; Itoh, T., Synthesis and Asymmetric Anionic Polymerization of Substituted 7-aryl-2, 6-dimethyl-1, 4-benzoquinone methides, *J. Polym. Sci., Part A: Polym. Chem.,* **2015**, *53*, 437-444.

(29) Yan, T.; Zhao, L.; He, M.; Soulé, J. F.; Bruneau, C.; Doucet, H., Reactivity of 3-Substituted Fluorobenzenes in Palladium-Catalysed Direct Arylations with Aryl Bromides, *Adv. Synth. Catal.,* **2014**, *356*, 1586-1596.

(30) Cyrański, M. K.; Klimentowska, P.; Rydzewska, A.; Serwatowski, J.; Sporzyński, A.; Stępień, D. K., Towards a Monomeric Structure of Phenylboronic Acid: The Influence of Ortho-Alkoxy Substituents on the Crystal Structure, *CrystEngComm,* **2012**, *14*, 6282-6294.

(31) Staroverov, V. N. *Density-Functional Approximations for Exchange and Correlation*; John Wiley & Sons, Inc., 2012.

(32) Earles, J. C.; Gordon, K. C.; Stephenson, A. W. I.; Partridge, A. C.; Officer, D. L., Spectroscopic and Computational Study of β-ethynylphenylene Substituted Zinc and Free-Base Porphyrins, *Phys. Chem. Chem. Phys.,* **2011**, *13*, 1597-1605.

(33) McCreery, R. L. *Raman Spectroscopy for Chemical Analysis*; Wiley, 2005.

(34) Wu, Z.; Fan, B.; Xue, F.; Adachi, C.; Ouyang, J., Organic Molecules Based on dithienyl-2,1,3-benzothiadiazole as New Donor Materials for Solution-Processed Organic Photovoltaic Cells, *Sol. Energy Mater. So. Cells,* **2010**, *94*, 2230-2237.

(35) Kato, S.-i.; Matsumoto, T.; Shigeiwa, M.; Gorohmaru, H.; Maeda, S.; Ishi-i, T.; Mataka, S., Novel 2,1,3-Benzothiadiazole-Based Red-Fluorescent Dyes with Enhanced Two-Photon Absorption Cross-Sections, *Chem. - Eur. J.,* **2006**, *12*, 2303-2317.

(36) Velusamy, M.; Justin Thomas, K.; Lin, J. T.; Hsu, Y.-C.; Ho, K.-C., Organic Dyes Incorporating Low-Band-Gap Chromophores for Dye-Sensitized Solar Cells, *Org. Lett.,* **2005**, *7*, 1899-1902.

(37) Wright, P. G.; Stein, P.; Burke, J. M.; Spiro, T. G., Resonance Raman Spectra, Excitation Profiles and Excited (Iron to Pyridine Charge Transfer) State Geometry of Bispyridine Iron(II) Heme, *J. Am. Chem. Soc.,* **1979**, *101*, 3531-3535.

(38) Horvath, R.; Gordon, K. C., Excited state vibrational spectroscopy of metal complexes of dipyrido [3, 2-a: 2′, 3′-c] phenazine, *Inorganica Chimica Acta,* **2011**, *374*, 10-18.

(39) Tawada, Y.; Tsuneda, T.; Yanagisawa, S.; Yanai, T.; Hirao, K., A Long-Range-Corrected Time-Dependent Density Functional Theory, *J. Chem. Phys.,* **2004**, *120*, 8425-8433.

(40) Peach, M. J. G.; Benfield, P.; Helgaker, T.; Tozer, D. J., Excitation Energies In Density Functional Theory: An Evaluation And a Diagnostic Test, *J. Chem. Phys.,* **2008**, *128*, 0-8.

(41) Li, Y.; Cao, Y.; Gao, J.; Wang, D.; Yu, G.; Heeger, A. J., Electrochemical Properties of Luminescent Polymers and Polymer Light-Emitting Electrochemical Cells, *Synth. Met.,* **1999**, *99*, 243-248.

(42) Strachan, C. J.; Pratiwi, D.; Gordon, K. C.; Rades, T., Quantitative Analysis of Polymorphic Mixtures of Carbamazepine by Raman Spectroscopy and Principal Components Analysis, *J. Raman Spectrosc.,* **2004**, *35*, 347-352.

(43) Kim, M. R.; Ma, D., Quantum-Dot-Based Solar Cells: Recent Advances, Strategies, and Challenges, *J. Phys. Chem. Lett.,* **2014**, *6*, 85-99.

(44) Shao, J.; Chang, J.; Chi, C., Linear and Star-Shaped Pyrazine-Containing Acene Dicarboximides With High Electron-Affinity, *Org. Biomol. Chem.,* **2012**, *10*, 7045-7052.

(45) Liu, Y.; Lu, Y.; Prashad, M.; Repič, O.; Blacklock, T. J., A Practical and Chemoselective Reduction of Nitroarenes to Anilines Using Activated Iron, *Adv. Synth. Catal.,* **2005**, *347*, 217-219.

(46) Frisch, M. J. e. a.; Gaussian Inc.: Wallingford, CT, 2009.

(47) Boyle, A., Tenderholt and KM Langner, *J. Comput. Chem,* **2008**, *29*, 839.

(48) Schaftenaar, G.; Noordik, J. H., Molden: a Pre- and Post-Processing Program for Molecular and Electronic Structures, *Journal of Computer-Aided Molecular Design*, *14*, 123-134.

(49) Gottlieb, H. E.; Kotlyar, V.; Nudelman, A., NMR Chemical Shifts of Common Laboratory Solvents as Trace Impurities, *J. Org. Chem,* **1997**, *62*, 7512-7515.

(50) CrysAlisPRO; Version 1.171.36.28 ed.; Agilent Technologies: Yarnton, Oxfordshire, UK, 2013.

(51) Sheldrick, G. M.; Programs for Crystal Structure Analysis: Göttingen, Germany, 1998.

(52) Sheldrick, G. M., A short history of SHELX, *Acta Crystallogr., Sect. A: Found. Adv.,* **2007**, *64*, 112-122.

(53) Horvath, R.; Gordon, K. C., Understanding Excited-State Structure in Metal Polypyridyl Complexes Using Resonance Raman Excitation Profiles, Time-Resolved Resonance Raman Spectroscopy and Density Functional Theory, *Coord. Chem. Rev.,* **2010**, *254*, 2505-2518.

(54) Nestor, J. R.; Lippincott, E. R., The Effect of the Internal Field on Raman Scattering Cross Sections, *J. Raman Spectrosc.,* **1973**, *1*, 305-318.

(55) Kato, Y.; Takuma, H., Absolute Measurement of Raman-Scattering Cross Sections of Liquids, *J. Opt. Soc. Am.,* **1971**, *61*, 347-350.

(56) Noviandri, I.; Brown, K. N.; Fleming, D. S.; Gulyas, P. T.; Lay, P. A.; Masters, A. F.; Phillips, L., The Decamethylferrocenium/Decamethylferrocene Redox Couple: A Superior Redox Standard to the Ferrocenium/Ferrocene Redox Couple for Studying Solvent Effects on the Thermodynamics of Electron Transfer, *J. Phys. Chem. B.,* **1999**, *103*, 6713-6722.

(57) Ali, A.; Liepa, A.; Thomas, M.; Wilkie, J.; Winzenberg, K., Preparation of Cyclohexane-1,3-dione Herbicide Precursors by Birch Reduction of 3,5-Dimethoxyphenyl-Substituted Silane Derivatives, *Aust. J. Chem.,* **1994**, *47*, 1205-1210.

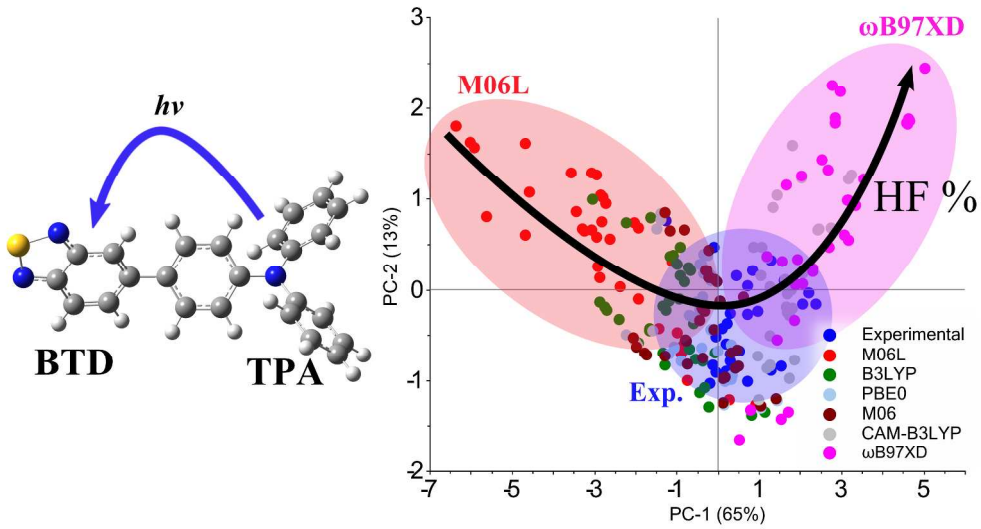

Predicting donor-acceptor properties: a systematic study of a series of donor-acceptor compounds in differing solvents reveal that electronic absorption properties are well modeled by the MO6 functional but Raman cross sections require range-separated functionals (CAM-B3LYP) for most accurate prediction.
254x137mm (300 x 300 DPI)